

Non-equilibrium scalar field dynamics starting from Fock states: Absence of thermalization in one dimensional phonons coupled to fermions

Md Mursalin Islam^{1,*} and Rajdeep Sensarma¹

¹*Department of Theoretical Physics, Tata Institute of Fundamental Research, Mumbai 400005, India.*

(Dated: July 19, 2022)

We propose a new method to study non-equilibrium dynamics of scalar fields starting from non-Gaussian initial conditions using Keldysh field theory. We use it to study dynamics of phonons coupled to non-interacting bosonic and fermionic baths, starting from initial Fock states. We find that in one dimension long wavelength phonons coupled to fermionic baths do not thermalize both at low and high bath-temperatures. At low temperature, constraints from energy-momentum conservation lead to a narrow bandwidth of particle-hole excitations and the phonons effectively do not see this bath. On the other hand, the strong band-edge divergence of the particle-hole density of states leads to an undamped polaritonlike mode of the dressed phonons above the band edge of the particle-hole excitations. These undamped modes contribute to the lack of thermalization of long wavelength phonons at high temperatures. In higher dimensions, these constraints and the divergence of density of states are weakened and lead to thermalization at all wavelengths.

I. INTRODUCTION

Scalar fields are paradigmatic degrees of freedom in quantum field theories, with wide ranging applications from particle physics to astro-particle physics and cosmology to condensed matter physics. In particle physics they played a big role in the construction of the Higgs mechanism, which leads to descriptions of massive particles¹⁻³. In cosmology and astro-particle physics, scalar fields have been used to describe inflationary expansion of the early universe^{4,5}; they have also been projected as possible candidates for dark matter in various models⁶⁻⁸. They are also ubiquitous in condensed matter physics, often rearing their heads as low energy fluctuations around ordered (symmetry broken) states of matter. From phonons in solids⁹ to magnons in certain types of magnets¹⁰ to phase fluctuations in a superfluid^{11,12}, there are a large variety of scalar fields which occur in descriptions of quantum many body systems. More recently, with the advent of technology to create strong light-matter interactions, photons in optical cavities¹³⁻¹⁶ or dressed excitations like polaritons¹⁷⁻²¹ can also be described by effective scalar fields.

Compared to the well developed equilibrium and ground state theory for scalar fields (including interacting field theories)²²⁻²⁴, the non-equilibrium dynamics of scalar fields are relatively less studied. The primary motivation for earlier studies of non-equilibrium dynamics of scalar fields was related to non-equilibrium processes in the early universe and in high energy collisions²⁵⁻²⁸. More recent advances in creating non-equilibrium states, either by pumping solid state systems with intense energy sources²⁹⁻³², or by pulse shaping³³⁻³⁷ and cavity engineering³⁸⁻⁴¹, has led to a renewed focus on this topic. In many of these cases, the system evolves starting from an athermal state. A typical example is a cavity where the photons are initiated to a squeezed state^{39,42-45}. Thus it is very important to obtain a description of dynamics of scalar fields starting from athermal initial conditions.

The standard Schwinger-Keldysh field theory used to describe non-equilibrium dynamics of many body systems, unfortunately requires a thermal initial condition to work^{24,46-50}. Recently Chakraborty et. al.⁵¹ looked at this problem for

Schrödinger bosons (fields obeying saddle point Schrödinger equation with single time derivatives). They found that arbitrary initial conditions can be incorporated in the field theory provided an additional source is coupled to the fields at the initial time. The correlators are calculated within this theory with the additional source. The physical correlation functions are then obtained by taking derivatives of these correlators with respect to the initial sources, with the set of derivatives determined by the initial conditions. In this paper, we extend this formalism to describe non-equilibrium dynamics of scalar fields starting from density matrices diagonal in occupation number (Fock) states. Other than having different symmetries, the key difference between Schrödinger bosons and scalar fields is that scalar fields obey a classical equation of motion which has 2^{nd} order time derivatives. Our formalism also requires additional sources at initial times. However, these sources couple to bilinears of both the initial fields and their time derivatives, reflecting the fact that the classical equations for these fields are now 2^{nd} order in time derivatives and require knowledge of both initial configurations and their time derivatives to be solved. The rest of the formalism is similar to Ref. 51; i.e. we calculate the correlators in presence of these sources and then take derivatives with respect to the initial sources to get physical correlation functions.

We use our formalism to study the thermalization of a system of scalar fields coupled to external baths, and initialized to athermal Fock states. Although we consider phonons as a concrete example in this case, similar considerations can be used for other scalar fields including complex ($O(2)$) and $O(N)$ scalar fields. We first consider coupling the phonons to a Markovian ohmic bath with a smooth ultra-violet cut-off⁵². Here, as expected, the phonons thermalize at a rate which becomes momentum independent as we go to the broad bandwidth limits of pure white noise⁵³.

We then consider the coupling of phonons with the particle-hole excitations of a non-interacting fermionic bath. The dynamics of electrons coupled to phonons has been extensively studied in the context of thermalization of “hot electrons”⁵⁴⁻⁶². Relatively less attention has been paid to the dynamics of the phonons coupled to fermions⁶³⁻⁶⁷. We note

that the evolution of one-particle distribution functions have been treated before using Kadanoff-Baym equations²⁷. In one dimension, at low temperatures, the density of particle-hole excitations with a fixed low momentum transfer is finite only over a narrow region of energy. In the long wavelength limit this almost reduces to a linearly dispersing mode with a width which scales quadratically with the momentum. As a result, the long wavelength phonon modes effectively do not see the fermionic bath as it is not possible to satisfy both energy and momentum conservation during exchange with the bath^{68,69}. Hence these modes undergo quantum oscillations and remember their initial occupation numbers even at very long times. These modes thus do not thermalize at low bath temperature. In principle two phonon scatterings, which occur at higher orders of system-bath couplings, do not suffer from the tight energy momentum conservation requirements. However we find that in presence of a Fermi sea, the decay rate of a phonon with energy ω_{ph} remains exponentially small ($\sim \omega_{ph} e^{-\frac{\omega_{ph}}{T}}$) for $T \ll \omega_{ph}$. For $T \gg \omega_{ph}$, we obtain a decay rate $\sim T$. This high T classical limit is similar to those considered in Refs.⁷⁰ and ⁷¹. The difference in the exponent between our results and earlier works^{70,71} comes from considering the fact that the relevant two-phonon process is mediated by a fermion with energy mismatch (i.e. off-shell) $\Delta\epsilon$, which scale with the momentum of the phonon which is decaying. Note that this is the dominant relaxation process for $\Delta\epsilon \gg T \gg \omega_{ph}$, while the relaxation is dominated by the single phonon process for $T \sim \Delta\epsilon$. We note that even higher order (8-th order in system-bath coupling) processes which involve two particle-hole excitations (three phonon processes), result in a decay rate which is polynomial in temperature and hence not exponentially small. But for small values of system-bath coupling these processes are highly suppressed.

At high temperatures, the particle-hole density of states extend from zero energy to a band maximum (due to a finite bandwidth of the fermions). An interesting feature of one dimensional fermions is a divergence in the single particle density of states at the upper edge of the corresponding band. This leads to a strong divergence in the particle-hole density of states near their band edge. This divergence in the bath density of states results in the formation of new dressed modes of the phonons just outside the upper band edge for the particle-hole excitations. This new mode, which we call a ‘‘polarinon’’ due to its similarity to polaritons formed by dressing of light with excitons^{72,73}, remains undamped, leading to the absence of thermalization of long-wavelength phonons, even at high bath temperatures. This is contrary to the general expectation that thermalization should be easier at high temperatures since energy-momentum constraints in scattering processes are relaxed. This new mode can be studied in one dimensional systems with strong electron-phonon coupling.

To contrast with the singular case of one dimensional particle-hole bath, we also consider a bath of two dimensional non-interacting electrons. In this case, there is no lower bound for the existence of particle-hole excitations and the phonons thermalize unless the Debye frequency of the phonons is larger than the bandwidth of the electrons. Further the singularities in the density of states of the particle-hole bath are

weakened, and hence there is no additional mode formation in this case. The scalar fields thermalize unless they are massive, which describes optical phonons in the present context. In that case, coupling to the Fermionic bath fails to thermalize the long wavelength phonons as energy-momentum constraints cannot be satisfied simultaneously.

We now provide a brief route map of the different sections of our paper. In section II, we set up the Keldysh field theory based formalism to describe non-equilibrium dynamics of scalar fields starting from Fock states. We initially work out the case of a single harmonic oscillator in section II A and extend it to the case of scalar fields in section II B. In section III we first set up the problem of dynamics of phonons coupled to external baths, where the phonons are initialized to a non-thermal Fock state. In section III A, we focus on the effects of a bosonic ohmic bath, while section III B 1 illustrates the example of a one dimensional fermionic bath, where the long wavelength phonons do not thermalize. We finish this section with the case of two dimensional fermionic bath in section III B 2. Finally we have summarized the results in the concluding section IV.

II. DYNAMICS WITH INITIAL CONDITIONS

Several problems in non-equilibrium dynamics relevant to different branches of physics require the description of dynamics of scalar fields starting from athermal initial conditions. Such initial conditions can result from sophisticated pulse-shaping techniques creating squeezed lights in optical cavities^{39,44,45}. They can also be created when a large amount of energy is dumped into a system with broken symmetry, as is done in the case of pump-probe experiments^{29–32,74–76}. This can also be relevant for high energy particles which can be created in non-equilibrium distributions due to particle collision/decay⁷⁷.

The standard textbook formalism of Schwinger-Keldysh field theory used to describe non-equilibrium dynamics however works when the initial condition is described by a thermal initial density matrix^{24,48–50}. In a recent paper, Chakraborty et. al⁵¹ had constructed a formalism to treat open system dynamics of bosons and fermions starting from arbitrary initial conditions. The bosons/fermions were described by a Schrödinger equation, which was suitably modified for open system dynamics. Here we will extend this formalism to the case of scalar fields whose classical equation of motion has 2^{nd} order time-derivative which brings additional complications. Before we describe the formalism for scalars, we first review the structure of the formalism put forward in Ref. 51. It will serve as a paradigm for comparing and contrasting the formalism developed here.

In Ref. 51 it was proposed that the athermal initial density matrix can be exponentiated by using a source term which allows it to be included in the action. In this formalism, the Schwinger-Keldysh action is modified by adding a source dependent action $\delta S(u)$ where the source u couples to the bilinears of the fields only at the initial time. The source only couple to the Keldysh ($q - q$) part of the action which carries

information about the initial state. For example, in the case of a single bosonic mode $\delta S(u) = i \frac{1+u}{1-u} \phi_q^*(0) \phi_q(0)$, when the system starts with an arbitrary initial density matrix $\rho_0 = \sum_n c_n |n\rangle \langle n|$ in the Fock basis. The correlation functions are calculated from the action with this extra source dependent part, which makes them dependent on the source u in general. The physical correlation functions \mathcal{G}_ρ are then calculated by taking a particular set of derivatives on the source dependent correlation functions $\mathcal{G}(u)$. This set of derivatives depends on the initial condition the system starts with. For the simple case of a single bosonic mode, $\mathcal{G}_\rho = \sum_n \frac{c_n}{n!} \partial_u^n \frac{1}{1-u} \mathcal{G}(u)|_{u=0}$. We will now extend the Schwinger-Keldysh field theory for scalar fields to include initial density matrices diagonal in Fock basis. We will first consider the case of a single harmonic oscillator in position basis which represents a single mode of scalar fields. Then we will generalize it for the scalar fields containing multiple modes.

A. The Case of a single Harmonic Oscillator

It is instructive to first consider the case of a single harmonic oscillator in the position basis. This will provide us with the basic structure of the theory, which can then be extended to real scalar fields. We consider the dynamics of a closed system of a one dimensional simple harmonic oscillator with frequency Ω , which is governed by the action

$$S = \int dt \frac{m}{2} \dot{x}^2 - \frac{1}{2} m \Omega^2 x^2. \quad (1)$$

We want to consider the dynamics of this system starting from the number or Fock states. However, in a harmonic oscillator (and similarly in scalar field theory), construction of the Fock states involves an additional energy scale. One can contrast this to Schrödinger theories, where one can define a Fock basis independent of any external scales. To see this, note that creation-annihilation operators defined by $a_\omega^\dagger = [\sqrt{\frac{m\omega}{\hbar}} \hat{x} - i \frac{\hat{p}}{\sqrt{\hbar m \omega}}] / \sqrt{2}$ and $a_\omega = [\sqrt{\frac{m\omega}{\hbar}} \hat{x} + i \frac{\hat{p}}{\sqrt{\hbar m \omega}}] / \sqrt{2}$ satisfy the standard bosonic algebra $[a_\omega, a_\omega^\dagger] = 1$ for any value of ω , and can be used to construct a complete number basis with non-negative integer eigenvalues. Unless $\omega = \Omega$, these states will not be the stationary states of our harmonic oscillator; nevertheless they can provide a complete basis to write the initial density matrix. This will allow us to consider density matrices which do not commute with the Hamiltonian of the system. In a closed system, this allows us to consider quench problems with non-trivial dynamics⁷⁸⁻⁸⁰. We will consider an initial density matrix which is diagonal in the number basis corresponding to a_ω operators, i.e.

$$\hat{\rho}_0 = \sum_n c_n |n_\omega\rangle \langle n_\omega|, \quad (2)$$

where $\sum_n c_n = 1$ for probability conservation. Shifting now to the Keldysh theory with doubled time contours (+ for forward propagation and - for backward propagation), the Keldysh partition function can be written as

$$Z = \int D[x_+] D[x_-] e^{i \int dt \frac{m}{2} (\dot{x}_+^2 - \dot{x}_-^2) - \frac{1}{2} m \Omega^2 (x_+^2 - x_-^2)} \langle x_+(0) | \hat{\rho}_0 | x_-(0) \rangle. \quad (3)$$

Using the Harmonic oscillator energy eigenfunctions, $\psi_n(x) = \langle x | n_\omega \rangle = \left(\frac{m\omega}{\pi}\right)^{\frac{1}{4}} \frac{1}{\sqrt{2^n n!}} e^{-\frac{1}{2} m \omega x^2} H_n(\sqrt{m\omega} x)$, where H_n are the Hermite polynomials (we have set $\hbar = 1$), the matrix element of the initial density matrix is given by

$$\begin{aligned} \langle x_+ | \hat{\rho}_0 | x_- \rangle &= \sqrt{\frac{m\omega}{\pi}} e^{-\frac{1}{2} m \omega (x_+^2 + x_-^2)} \sum_n \frac{c_n}{2^n n!} H_n(\sqrt{m\omega} x_+) H_n(\sqrt{m\omega} x_-) \\ &= \sqrt{\frac{m\omega}{\pi}} \sum_n \frac{c_n}{n!} \frac{\partial^n}{\partial u^n} \frac{1}{\sqrt{1-u^2}} e^{m\omega f(u) x_+ x_- - \frac{1}{2} m \omega g(u) (x_+^2 + x_-^2)} \Big|_{u=0}, \end{aligned} \quad (4)$$

where $f(u) = \frac{2u}{1-u^2}$, $g(u) = \frac{1+u^2}{1-u^2}$, and we have used the Mehler formula⁸¹ for the generating function of products of Hermite polynomials to obtain the last expression.

One can now write the partition function describing the dynamics starting from this initial condition as

$$Z = \tilde{\mathcal{L}}(\partial_u, \rho_0) Z(u) \Big|_{u=0}, \quad (5)$$

where the differential operator $\tilde{\mathcal{L}} = \sum_n \frac{c_n}{n!} (\partial_u)^n \frac{1}{\sqrt{1-u^2}}$ depends on the initial density matrix. It is useful to write $\tilde{\mathcal{L}} = \mathcal{L} \mathcal{M}(u)$, where $\mathcal{L} = \sum_n \frac{c_n}{n!} (\partial_u)^n$ and $\mathcal{M}(u) = \frac{1}{\sqrt{1-u^2}}$. Here, the partition function in presence of source terms at the initial time is

$Z(u) = \sqrt{m\omega/\pi} \int D[x_+]D[x_-]e^{iS(u)}$, where

$$S(u) = -\frac{m}{2} \int dt \int dt' (x_+(t), x_-(t)) \begin{pmatrix} \delta(t-t')(\partial_t^2 + \Omega^2) & i\omega f(u)\delta(t)\delta(t') \\ +\delta(t)\delta(t')[\partial_{t'} - i\omega g(u)] & \\ i\omega f(u)\delta(t)\delta(t') & \delta(t-t')(-\partial_t^2 - \Omega^2) \\ & -\delta(t)\delta(t')[\partial_{t'} + i\omega g(u)] \end{pmatrix} \begin{pmatrix} x_+(t') \\ x_-(t') \end{pmatrix}. \quad (6)$$

Note that in addition to the source terms related to imposing the correct initial condition on the dynamics, there is an additional time derivative term at $t = 0$. This boundary term comes from an integration by parts, which converts $\dot{x}^2 \rightarrow x\ddot{x}$ in the action and is ignored in theories where the time co-ordinate extends up-to $-\infty$. As a simple check, one can easily show that without any additional sources present, $Z(u) = \sqrt{\frac{1+u}{1-u}}$, and hence $Z = \sum_n c_n = 1$, as one expects for the Keldysh partition function.

The correlation functions in this theory can be calculated by adding sources coupling linearly to x at arbitrary times and

taking derivatives with respect to these sources. The derivatives with respect to these linear sources commute with the derivatives with respect to the bilinear initial source u . Hence one can write

$$D(\rho_0) = \mathcal{L}(\partial_u, \rho_0)\mathcal{N}(u)D(u)|_{u=0} \quad (7)$$

where $D(\rho_0)$ is the correlator corresponding to the physical dynamics with the initial condition, while $D(u)$ is the correlation function in the theory with the initial sources. The normalization $\mathcal{N}(u) = \mathcal{M}(u)Z(u) = \frac{1}{1-u}$. Focussing on the single particle Green's function, we can invert the matrix in Eq. (6) to write

$$\begin{aligned} D^{+-}(t, t', u) &= \frac{1}{2m\Omega} \sin \Omega(t-t') - \frac{i}{2m\omega} \frac{1+u}{1-u} \left\{ \cos \Omega t \cos \Omega t' + \frac{\omega^2}{\Omega^2} \sin \Omega t \sin \Omega t' \right\} \\ D^{-+}(t, t', u) &= \frac{-1}{2m\Omega} \sin \Omega(t-t') - \frac{i}{2m\omega} \frac{1+u}{1-u} \left\{ \cos \Omega t \cos \Omega t' + \frac{\omega^2}{\Omega^2} \sin \Omega t \sin \Omega t' \right\} \\ D^{++}(t, t', u) &= \Theta(t-t')D^{-+}(t, t', u) + \Theta(t'-t)D^{+-}(t, t', u) \text{ and} \\ D^{--}(t, t', u) &= \Theta(t-t')D^{+-}(t, t', u) + \Theta(t'-t)D^{-+}(t, t', u). \end{aligned} \quad (8)$$

The details of this calculation are presented in Appendix A.

It is useful to work with the Keldysh rotated classical $x_{cl} = \frac{1}{2}(x_+ + x_-)$ and the quantum $x_q = \frac{1}{2}(x_+ - x_-)$ degrees of freedom. In this basis, the one particle Green's functions take the form

$$\hat{D} = \begin{pmatrix} D^K & D^R \\ D^A & 0 \end{pmatrix}, \quad (9)$$

with

$$\begin{aligned} D^R(t, t', u) &= -\Theta(t-t') \frac{\sin \Omega(t-t')}{2m\Omega} = D^A(t', t, u) \text{ and} \quad (10) \\ D^K(t, t', u) &= -\frac{i}{2m\omega} \frac{1+u}{1-u} \left[\cos \Omega t \cos \Omega t' + \frac{\omega^2}{\Omega^2} \sin \Omega t \sin \Omega t' \right] \\ &= -2im\omega \frac{1+u}{1-u} D^R(t, \epsilon) \left[1 + \frac{1}{\omega^2} \overleftarrow{\partial}_\epsilon \overrightarrow{\partial}_\epsilon \right] D^A(\epsilon, t') \Big|_{\epsilon=0}. \end{aligned}$$

We find that the retarded (and advanced) Green's functions are independent of the initial conditions/ initial sources, while the Keldysh Green's function depends on them. It is then easy to show that the retarded Green's function for the actual dynamics starting from the initial condition has the same form as in Eq. (10), while the physical Keldysh Green's function is given by

$$D^K(t, t', \rho_0) = -2im\omega \sum_n c_n (1+2n) D^R(t, \epsilon) \left[1 + \frac{1}{\omega^2} \overleftarrow{\partial}_\epsilon \overrightarrow{\partial}_\epsilon \right] D^A(\epsilon, t') \Big|_{\epsilon=0}. \quad (11)$$

One can now write the action in the Keldysh rotated basis including the source terms, which will reproduce the correlators

$$S = -m \int dt \int dt' (x_{cl}(t), x_q(t)) \begin{pmatrix} 0 & \delta(t-t')(\partial_t^2 + \Omega^2) \\ \delta(t-t')(\partial_t^2 + \Omega^2) & -i\omega \frac{1+u}{1-u} \left[\delta(t)\delta(t') + \frac{1}{\omega^2} \overleftarrow{\partial}_t \delta(t)\delta(t') \overrightarrow{\partial}_{t'} \right] \end{pmatrix} \begin{pmatrix} x_{cl}(t') \\ x_q(t') \end{pmatrix}. \quad (12)$$

Note that in continuum, it is preferable to do a Keldysh rotation on the correlators in \pm basis to get the correlators in $cl - q$ basis and then write an action in the $cl - q$ basis which reproduces the correct correlators. A direct field rotation on the continuum action Eq. (6) does not reproduce Eq. (12). This is a well-known problem in standard Keldysh field theory in continuum, which does not appear in discrete time versions⁴⁹. The steps outlined here correctly reproduces all correlators in the system.

We note that the structure of the action is similar to that obtained for a Schrödinger theory of bosons, i.e. we add a bilinear source u which couples only to the quantum fields at the initial time. This anti-Hermitian term effectively acts as a Keldysh self energy for the fields. However, there is one key difference: unlike the Schrödinger bosons, where the u terms are only coupled to bilinears of the fields at $t = 0$, here the additional terms couple both to the position and its time-derivatives at the initial time. This is a reflection of the fact that the saddle point equation is second order in time in this case and both the initial position and the initial velocity of the particle are required to solve this equation.

There is an alternate way of deriving the effective action Eq. (12). One can start with the coherent state representation of the harmonic oscillator and using the theory derived in

Ref. 51, derive the effective action in the Keldysh rotated basis of complex Schrödinger bosons. One can then write the coherent state fields in terms of position and momentum degrees of freedom in a path integral on the phase space. Integrating out the momentum degrees of freedom, one can arrive at the effective action derived above. In this case, it is easy to see that the initial sources couple to both position and momentum, and hence, on integrating out the momentum degrees of freedom, they couple to the time derivative of the position at initial times. We note that this derivation works when ω and Ω are same, while the detailed derivation provided in this paper also works even when the Fock states of the initial density matrix are not the eigenstates of the closed system dynamics.

Before we move to the case of the scalar fields, we need to discuss how the dynamics changes if the system is coupled to an external bath starting at $t = 0$, leading to open quantum system dynamics. The addition of a bath (at least the simplest baths where the position of the oscillator couples to the bath degrees of freedom), leads to a quadratic theory where the effect of the bath can be incorporated through a retarded self-energy Σ^R and a Keldysh self-energy Σ^K , corresponding respectively to dissipative and stochastic effects of the bath. The Keldysh self energy simply adds to the initial self-energy from the bilinear sources, so the correlators in presence of the external bath are given by

$$D^R(t-t') = D_0^R(t-t') + \int_{t'}^t dt_1 \int_{t'}^{t_1} dt_2 D_0^R(t-t_1) \Sigma^R(t_1-t_2) D^R(t_2-t') \quad (13)$$

$$D^K(t, t', \rho_0) = -2im\omega \sum_n c_n (1+2n) D^R(t, \epsilon) \left[1 + \frac{1}{\omega^2} \overleftarrow{\partial}_\epsilon \overrightarrow{\partial}_\epsilon \right] D^A(\epsilon, t') \Big|_{\epsilon=0} + \int_0^t dt_1 \int_0^{t'} dt_2 D^R(t-t_1) \Sigma^K(t_1, t_2) D^A(t_2-t'),$$

where $D_0^R(t-t')$ is the retarded correlator in absence of the bath (given by Eq. 10).

Finally, we note that one can introduce effects of interaction by adding an interaction term in the Keldysh action. In this case, the dynamics is not exactly solvable, and one needs to make approximations to treat effects of interaction on the open system dynamics. It is important to note that even in this case, one can use standard diagrammatic techniques for calculating $D(u)$, and then obtain $D(\rho_0)$ by taking appropriate derivatives.

B. Scalar Fields

We would now like to extend our formalism to the dynamics of scalar fields. In this paper, we will discuss the case of real scalar fields for the sake of brevity, but the formalism can be extended to complex scalar fields, or to $O(N)$ fields in a straightforward way. We consider real scalar fields $\phi(\mathbf{x}, t)$, whose dynamics is governed by the action

$$S = \int dt \int d^d x (\phi_{cl}(\mathbf{x}, t), \phi_q(\mathbf{x}, t)) \begin{pmatrix} 0 & -\partial_t^2 + c^2 \nabla^2 - m^2 \\ -\partial_t^2 + c^2 \nabla^2 - m^2 & 0 \end{pmatrix} \begin{pmatrix} \phi_{cl}(\mathbf{x}, t) \\ \phi_q(\mathbf{x}, t) \end{pmatrix}. \quad (14)$$

Working with momenta instead of real space, this gives

$$S = \int dt \int d^d k (\phi_{cl}(-\mathbf{k}, t), \phi_q(-\mathbf{k}, t)) \begin{pmatrix} 0 & -\partial_t^2 - \Omega_{\mathbf{k}}^2 \\ -\partial_t^2 - \Omega_{\mathbf{k}}^2 & 0 \end{pmatrix} \begin{pmatrix} \phi_{cl}(\mathbf{k}, t) \\ \phi_q(\mathbf{k}, t) \end{pmatrix}, \quad (15)$$

where $\Omega_{\mathbf{k}} = \sqrt{c^2 \mathbf{k}^2 + m^2}$ is the dispersion of a generic massive scalar field. One can of course set $m = 0$ to describe massless scalar fields. We note that since the theory would be written in terms of $\Omega_{\mathbf{k}}$, one can also put the system on a lattice and consider

lattice dispersions with associated finite range of lattice momenta (Brillouin zones).

We assume that the system is initialized to a density matrix which is diagonal in the Fock basis of the number operators $\hat{n}_{\mathbf{k}} = a_{\mathbf{k}}^\dagger a_{\mathbf{k}}$, where $a_{\mathbf{k}} = \sqrt{\frac{\omega_{\mathbf{k}}}{2}} \phi(\mathbf{k}) + i\sqrt{\frac{1}{2\omega_{\mathbf{k}}}} \dot{\phi}(\mathbf{k})$. Here $\omega_{\mathbf{k}}$ is a dispersion which can be different from $\Omega_{\mathbf{k}}$, and hence the initial state may not be an eigenstate of the Hamiltonian which

$$S = \int dt \int dt' \int d^d k (\phi_{cl}(-\mathbf{k}, t), \phi_q(-\mathbf{k}, t)) \begin{pmatrix} 0 & \delta(t-t')(-\partial_t^2 - \Omega_{\mathbf{k}}^2) \\ \delta(t-t')(-\partial_t^2 - \Omega_{\mathbf{k}}^2) & i\omega_{\mathbf{k}} \frac{1+u_{\mathbf{k}}}{1-u_{\mathbf{k}}} \left[\delta(t)\delta(t') + \frac{1}{\omega_{\mathbf{k}}^2} \overleftarrow{\partial}_t \delta(t) \delta(t') \overrightarrow{\partial}_{t'} \right] \end{pmatrix} \begin{pmatrix} \phi_{cl}(\mathbf{k}, t') \\ \phi_q(\mathbf{k}, t') \end{pmatrix}. \quad (16)$$

We consider a system starting from $\rho_0 = \sum_{\{n\}} c_{\{n\}} |\{n\}\rangle \langle \{n\}|$. The physical correlation functions for

$$D^R(\mathbf{k}; t-t') = D_0^R(\mathbf{k}; t-t') + \int_{t'}^t dt_1 \int_{t'}^{t_1} dt_2 D_0^R(\mathbf{k}; t-t_1) \Sigma^R(\mathbf{k}; t_1-t_2) D^R(\mathbf{k}; t_2-t') \quad (17)$$

$$D^K(\mathbf{k}; t, t', \rho_0) = -2i\omega_{\mathbf{k}} \sum_{\{n\}} c_{\{n\}} (1+2n_{\mathbf{k}}) D^R(\mathbf{k}; t, \epsilon) \left[1 + \frac{1}{\omega_{\mathbf{k}}^2} \overleftarrow{\partial}_\epsilon \overrightarrow{\partial}_\epsilon \right] D^A(\mathbf{k}; \epsilon, t') \Big|_{\epsilon=0} + \int_0^t dt_1 \int_0^{t_1} dt_2 D^R(\mathbf{k}; t-t_1) \Sigma^K(\mathbf{k}; t_1, t_2) D^A(\mathbf{k}; t_2-t'),$$

where $\Sigma^R(\mathbf{k}; t-t')$ and $\Sigma^K(\mathbf{k}; t, t')$ are retarded self-energy and Keldysh self-energy respectively for each mode. The self energies can arise if the system is coupled to an external bath, or from the interaction between the modes of the scalar fields. We will now use this formalism to study the non-equilibrium dynamics of scalar fields coupled to external baths. While this formalism is valid for any scalar fields, we will look into the concrete example of phonons coupled to various kinds of external baths to illustrate the use of this formalism.

III. DYNAMICS OF PHONONS COUPLED TO EXTERNAL BATH

We now consider the dynamics of a system of phonons (quantized lattice vibrations) initialized to a non-thermal state and coupled to an external bath. In one dimension, the bare dispersion of the phonons is given by

$$\Omega_k = \sqrt{\omega_0^2 \sin^2(ka/2) + m^2}, \quad (18)$$

where a is the lattice spacing and m is the mass, which can be set to 0 to describe longitudinal phonons. For the massless phonons, the long wavelength modes have a linear dispersion $\Omega_k \sim c_s k$, with the sound velocity $c_s = \frac{\omega_0 a}{2}$. Since

generates the dynamics of the system.

In this case, we can generalize the answers we obtained for the simple harmonic oscillator in a straightforward way. The source u is generalized to a source field $u_{\mathbf{k}}$ for each mode \mathbf{k} and the source dependent action in the Keldysh basis is

this dynamics is given by

we are working on a lattice, the Brillouin zone extends from $k = -\pi/a$ to $k = \pi/a$. The bandwidth of the massless phonons is then given by ω_0 , which controls both the ultraviolet and the infrared dispersions in this simple model. We also note that this kind of dispersion is not specific to phonons, there exist other systems (for example magnons or quantized spin waves), which can be described by similar scalar field dispersion. The massive fields, which can be used to represent optical phonons, have a low energy dispersion $\Omega_k \sim \sqrt{c_s^2 k^2 + m^2} \sim m + \frac{k^2}{2m^*}$, where the curvature $m^* \sim m/c_s^2$.

In two dimensions, we consider phonons on a square lattice of lattice spacing a , with the bare dispersion given by

$$\Omega_{\mathbf{k}} = \sqrt{\omega_0^2 [\sin^2(k_x a/2) + \sin^2(k_y a/2)] + m^2}. \quad (19)$$

Once again, for the massless scalar fields, the long wavelength modes have a linear dispersion $\Omega_{\mathbf{k}} \sim c_s |\mathbf{k}|$, with speed $c_s = \frac{\omega_0 a}{2}$, while for the massive fields, the low energy dispersion $\Omega_{\mathbf{k}} \sim \sqrt{c_s^2 \mathbf{k}^2 + m^2} \sim m + \frac{\mathbf{k}^2}{2m^*}$, where m^* has the same form as in the one dimensional case. We note that for a square lattice, the Brillouin zone extends from $k_x = -\pi/a$ to $k_x = \pi/a$ and $k_y = -\pi/a$ to $k_y = \pi/a$.

We study the dynamics of these phonon modes starting

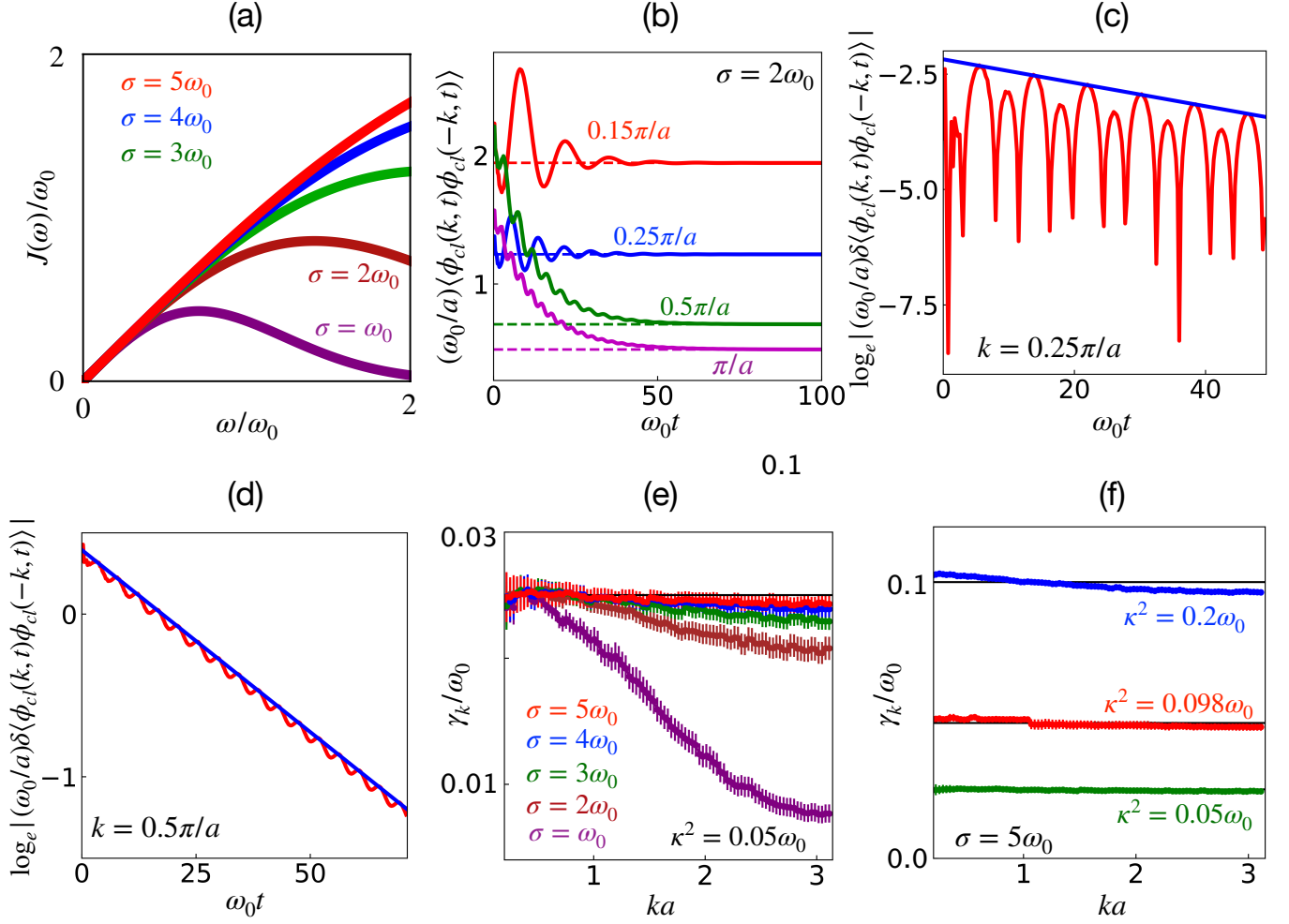


FIG. 1. Non-equilibrium dynamics of phonons coupled to an ohmic bath: (a) The bath spectral function $J(\omega) = \omega e^{-\frac{\omega^2}{\sigma^2}}$ as a function of ω for different values of σ . Here ω_0 is the bandwidth of bare phonons. $J(\omega)$ deviates from linear behaviour at progressively smaller energies as σ is decreased. (b) Thermalizing dynamics of correlation function $iD^K(k; t, t)$ for four different momentum modes at a low temperature $T = 0.02\omega_0$ with system-bath coupling strength $\kappa^2 = 0.05\omega_0$. Here $\sigma = 2\omega_0$. The time dependent correlation functions (solid lines) relax to their thermal values (dashed lines) at long times. (c) and (d) Difference of the time dependent correlation function and its thermal value as a function of time in a log plot for two momentum modes, (c) $k = 0.25\pi/a$, whose initial occupation is 0 and (d) $k = 0.5\pi/a$, whose initial occupation is 1. The decay rate is extracted from the slope of the envelope in the log plot. (e) Decay rate (γ_k) versus momentum (k) for different values of the effective bath bandwidth σ . γ_k approaches the constant value $\kappa^2/2$ independent of k as σ/ω_0 is increased and the bath approaches the limit of pure white noise. (f) Decay rate (γ_k) versus momentum (k) for different values of system bath coupling. σ is fixed at the highest value $5\omega_0$ we considered. We see that γ_k goes very close to the constant value $\kappa^2/2$. Note that with increasing system bath coupling, γ_k starts to have a weak k dependence.

from an athermal initial condition. Since the coupling to the bath will anyway generate non-trivial dynamics, we consider the initial state of the system to be a Fock state corresponding to the bare phonon dispersion $\Omega(\mathbf{k})$ i.e. we consider the annihilation operator $a_{\mathbf{k}} = \sqrt{\frac{\Omega_{\mathbf{k}}}{2}}\phi(\mathbf{k}) + i\sqrt{\frac{1}{2\Omega_{\mathbf{k}}}}\dot{\phi}(\mathbf{k})$ and the occupation number states corresponding to $\hat{n}_{\mathbf{k}} = a_{\mathbf{k}}^\dagger a_{\mathbf{k}}$. In one dimension, we consider a lattice of even number of sites $2L$ with momenta $k = \pm\pi i/L$ with integer i . The initial Fock state then corresponds to $n_k = 1$ for even values of i and 0 for odd values of i . Similarly in two dimensions we consider a square lattice of $(2L)^2$ sites with momenta

$(k_x, k_y) = (\pm\pi i/L, \pm\pi j/L)$ with integer i and j . The initial Fock state then corresponds to $n_{\mathbf{k}} = 1$ for even values of i and $n_{\mathbf{k}} = 0$ for odd values of i , so we have strips of occupation numbers 0 and 1 along the y -axis. These states are quite different from a thermal state of the bosons. The thermal state has a large occupancy near $\mathbf{k} = (0, 0)$ which decreases monotonically as \mathbf{k} is increased. The main broad features of the dynamics, like presence/absence of thermalization or the rates of thermalization, do not depend on this particular choice of initial state. However, details of phase oscillations in systems that do not thermalize will depend on the initial conditions. The initial conditions are chosen to provide a simple system

to distinguish between the modes that thermalize versus the modes that do not thermalize. We will now consider different kinds of baths and study their effects on the dynamics of the phonons.

A. Phonons Coupled to an Ohmic Bath

We first consider phonons in one dimension coupled to a bosonic bath. The effect of the bath on the phonons is controlled by the bath spectral function $J(\omega)$. Here we consider the case where all the phonon modes see the same ohmic bath with $J(\omega) = \omega e^{-\frac{\omega^2}{\sigma^2}}$. This bath spectral function is linear in energy for low ω ($\ll \sigma$) which is characteristic of the ohmic bath^{52,82}. The parameter σ ensures that the bath is well behaved in the ultra-violet limit with the spectral function smoothly decaying to zero at large energy. So σ plays the role of an effective bandwidth for the bath without producing non-analyticities which lead to non-Markovian dynamics⁸³. The bath spectral function $J(\omega)$ is plotted as a function of energy for five different values of σ ranging from $\sigma = \omega_0$ to $\sigma = 5\omega_0$ in Fig. 1(a). It is clear that the bath spectral function deviates from its linear behaviour at progressively lower energies as σ is decreased. We note that we have absorbed certain constants into the system bath coupling here, so that both κ^2 and $J(k, \omega)$ have dimensions of energy in this problem.

In this case, the momentum independent retarded self energy is given by

$$\Sigma^R(\omega) = -\kappa^2 \int_{-\infty}^{\infty} \frac{dz}{2\pi} J(z) \left[\frac{1}{z - \omega - i0^+} + \frac{1}{z + \omega + i0^+} \right]. \quad (20)$$

Note that $Im \Sigma^R(\omega) = -\kappa^2 J(\omega)$ and $Re \Sigma^R(\omega) = -\frac{\kappa^2}{\sqrt{\pi}} \left[\sigma - 2\omega F_D\left(\frac{\omega}{\sigma}\right) \right]$, where $F_D(x) = e^{-x^2} \int_0^x dy e^{y^2}$ is the Dawson's function⁸⁴.

The Keldysh self energy is

$$\Sigma^K(\omega) = -i\kappa^2 2 \coth\left(\frac{\omega}{2T}\right) J(\omega), \quad (21)$$

which follows from fluctuation-dissipation theorem⁴⁹. Here T is the temperature of the bath.

If the effective bandwidth of the bath σ is much larger than the phonon bandwidth ω_0 , then all the phonon modes effectively see a Gaussian white noise and one would expect the modes to thermalize at the same rate $\gamma = \kappa^2/2$. On the other hand, if σ is less than or comparable to ω_0 then the relaxation of different phonon modes depends on their energies with the slowest relaxation rate for the highest phonon energy. To see this, we track the dynamics of the phonons coupled to this ohmic bath ($T = 0.2\omega_0$ and $\sigma = 2\omega_0$) with a system-bath coupling strength $\kappa^2 = 0.05\omega_0$. In Fig. 1(b), we plot the time evolution of the correlation function $\langle \phi_{cl}(k, t) \phi_{cl}(-k, t) \rangle$ for four different values of momentum k . The correlation function decays to its thermal value with damped oscillations. While the steady state is independent of the initial condition, the modes which are initially populated approach the steady value from above while the correlation in the unpopulated

modes oscillate around the long time value. We plot the absolute value of the deviation of the correlation function from its steady value on a log scale for $k = 0.25\pi/a$ ($n_k = 0$ at $t = 0$) in Fig. 1(c) and for $k = 0.5\pi/a$ ($n_k = 1$ at $t = 0$) in Fig. 1(d). An exponential fit to the envelope of such curves is used to determine the momentum dependent decay rate γ_k . In Fig. 1(e), we plot γ_k as a function of k for the five different bath bandwidths ranging from $\sigma = \omega_0$ to $\sigma = 5\omega_0$. For $\sigma = \omega_0$ we find that the decay rate strongly depends on k , decreasing by a factor of 2.5 as we go from the zone centre to the edge of the Brillouin zone. As σ is increased, the dependence of γ_k on k is weakened with an almost k -independent γ for $\sigma = 5\omega_0$. The large bandwidth bath thus behaves like a source of Gaussian white noise⁵³. In the large bandwidth limit, we consider the effect of the system bath coupling on the decay rate γ in Fig. 1(f). As expected, the system decays faster as system bath coupling is increased. We note that with increasing system bath coupling γ acquires a weak k -dependence even for $\sigma = 5\omega_0$.

B. Phonons Coupled to a Fermionic Bath

We now consider the dynamics a system of scalar fields initialized to a Fock state and coupled to a bath of non-interacting fermions. This is prototype of a system which can be found in varied contexts in nature, like phonons coupled to electrons⁸⁵⁻⁸⁷, light coupled to metallic systems^{88,89}, ultracold atoms in cavity⁹⁰, descriptions of early universe and multi-component dark matter systems⁹¹. For concreteness, we will consider phonons coupled to non-interacting fermions.

We consider a bath of non-interacting spinless fermions with a Hamiltonian given by

$$H_F = \sum_{\mathbf{k}} \epsilon_{\mathbf{k}} \psi^\dagger(\mathbf{k}) \psi(\mathbf{k}), \quad (22)$$

where $\psi(\mathbf{k})$ are the fermion annihilation operators in mode \mathbf{k} and $\epsilon_{\mathbf{k}}$ is the corresponding dispersion. We consider fermions hopping on a linear chain in one dimension and on a square lattice in two dimensions with only nearest neighbour hopping, which results in the dispersions $\epsilon_{\mathbf{k}} = -\epsilon_B \cos ka$ and $\epsilon_{\mathbf{k}} = -\epsilon_B [\cos k_x a + \cos k_y a]$ respectively, where a is the lattice constant. Here, the bandwidth of the fermions is given by $2\epsilon_B$ (1-D) and $4\epsilon_B$ (2-D) respectively. The fermionic bath is characterized by a temperature T and a chemical potential μ , which fixes the particle density in the bath.

The phonons couple to the fermionic bath through the Hamiltonian

$$H_{int} = \kappa \sum_{\mathbf{k}, \mathbf{q}} \lambda(\mathbf{k}) \psi^\dagger(\mathbf{k} + \mathbf{q}) \psi(\mathbf{q}) \phi(\mathbf{k}), \quad (23)$$

where κ is the system bath coupling strength and the form factor $\lambda(\mathbf{k}) = \sqrt{\sum_{j=1}^D \sin^2(k_j a/2)}$ is related to the deformation potential acting between electrons and phonons⁹². Here $\phi(q)$ has the dimension of $[\sqrt{\text{volume/energy}}]$, while $\psi(k)$ has the dimension of $\sqrt{\text{volume}}$, hence κ^2 has the dimension of

[energy]³ × volume. We would like to note that the system bath coupling in this problem has different dimensions than in the problem with the ohmic bath.

The non-unitary dynamics of the phonons is governed by the retarded self energy $\Sigma^R(\mathbf{k}; t - t')$ and the Keldysh self energy $\Sigma^K(\mathbf{k}; t, t')$. The real part of Σ^R leads to the dressing of phonon dispersion while its imaginary part controls the dissipation in the system. The Keldysh self energy Σ^K controls the stochastic noise from the external bath. It is clear from Eq. (23) that the phonons actually couple to the particle-hole excitations of the fermionic system. The retarded self energy is then given by,

$$\Sigma^R(\mathbf{k}, \omega) = \kappa^2 \lambda(\mathbf{k})^2 \sum_{\mathbf{q}} \frac{F(\epsilon_{\mathbf{k}+\mathbf{q}}) - F(\epsilon_{\mathbf{q}})}{\omega + i\eta + \epsilon_{\mathbf{q}} - \epsilon_{\mathbf{k}+\mathbf{q}}}, \quad (24)$$

where $F(x) = \tanh\left(\frac{x-\mu}{2T}\right)$ (see Appendix B for a derivation). The imaginary part of Σ^R , which controls the dissipation in the system, is related to the spectral function of the effective bath $J(\mathbf{k}, \omega)$ by

$$\begin{aligned} \text{Im}[\Sigma^R(\mathbf{k}, \omega)] &= -\kappa^2 J(\mathbf{k}, \omega) \\ &= -\pi \kappa^2 \lambda(\mathbf{k})^2 \sum_{\mathbf{q}} \delta(\omega - \epsilon_{\mathbf{k}+\mathbf{q}} + \epsilon_{\mathbf{q}}) [F(\epsilon_{\mathbf{k}+\mathbf{q}}) - F(\epsilon_{\mathbf{q}})]. \end{aligned} \quad (25)$$

Using fluctuation-dissipation theorem, the Keldysh self energy is given by

$$\begin{aligned} \Sigma^K(\mathbf{k}, \omega) &= 2i \coth\left(\frac{\omega}{2T}\right) \text{Im}[\Sigma^R(\mathbf{k}, \omega)] \\ &= i2\pi \kappa^2 \lambda(\mathbf{k})^2 \sum_{\mathbf{q}} \delta(\omega - \epsilon_{\mathbf{k}+\mathbf{q}} + \epsilon_{\mathbf{q}}) [F(\epsilon_{\mathbf{k}+\mathbf{q}})F(\epsilon_{\mathbf{q}}) - 1]. \end{aligned} \quad (26)$$

For the non-equilibrium evolution of the phonon correlator, we find it easier to construct the retarded Green's function in frequency space, $D^R(\mathbf{k}, \omega) = \frac{1}{2[(\omega+i0^+)^2 - \Omega_{\mathbf{k}}^2] - \Sigma^R(\mathbf{k}, \omega)}$ and then Fourier transform $D^R(\mathbf{k}, \omega)$ and $i\omega D^R(\mathbf{k}, \omega)$ to get $D^R(\mathbf{k}, t - t')$ and its derivatives. $\Sigma^K(\mathbf{k}, \omega)$ is Fourier transformed to get $\Sigma^K(\mathbf{k}, t - t')$. The integrals for the Dyson equation for $D^K(\mathbf{k}, t, t)$ [Eq. (17)] are then performed numerically to obtain the physical correlators.

The particle-hole excitations, to which the scalar fields couple, have qualitatively different density of states (DOS) in one and two dimensions. This difference is reflected in the dynamics of the scalar fields through the self-energies. So, we will consider the case of one and two dimensional systems separately.

1. One dimensional systems

There are two reasons why one dimensional systems show atypical behaviour: (a) energy-momentum conservation relations impose tight constraints on possible processes in one dimension and (b) the density of states of excitations have strong

singular behaviour in one dimension. As we will see in this section, both these factors play an important role in the absence of thermalization for long wavelength phonons in one dimension.

To understand the novel behaviour of the system, we focus on the polarization function of a one dimensional free Fermi gas. We first consider $T = 0$. In Fig. 2(a), the region in the $k - \omega$ plane where $J(k, \omega)$ is finite at $T = 0$ is shown as a shaded region bounded by solid lines. The upper limit is given by the curves $\omega = (v_F/a) \sin ka + \mu(1 - \cos ka)$ for $k \leq |2k_F - \pi|$ and $\omega = 2\epsilon_B \sin(ka/2)$ for $k > |2k_F - \pi|$, while the lower limit is given by $\omega = (v_F/a) \sin ka - \mu(1 - \cos ka)$ for $k \leq 2k_F$ and $\omega = -(v_F/a) \sin ka + \mu(1 - \cos ka)$ for $k > 2k_F$, where k_F is the Fermi wave-vector of the Fermions and v_F is the Fermi velocity. At low momenta, both the upper and lower limits $\sim v_F k$, and thus the region actually merges into a single line with a slope of v_F . For the particle-hole symmetric point at half-filling ($\mu = 0$), the collapse of upper and lower limits is exact for low k . As we move away from half-filling, the width of the region at low $k \sim (\mu a^2/2)k^2$. This is a consequence of the strong constraints of energy and momentum conservation in one dimension. In this case, the long-wavelength phonons will not see any bath and undergo unitary quantum dynamics unless the phonon velocity c_s is exactly equal to v_F . Note that, in an interacting system, where one would expect a Luttinger liquid like behaviour⁹³, one would once again get a linearly dispersing mode with the velocity tuned by the Luttinger parameter. Further, at low temperatures, the particle-hole spectral weight outside this region is exponentially small. Since this fine tuning ($v_F = c_s$) is impossible in real systems, the long wavelength phonons will not thermalize at low temperature in one dimension. More precisely, for $T \ll c_s q$, the thermalization timescale will be exponentially large in inverse temperature ($\tau^{-1} \sim e^{-\frac{(v_F - c_s)k}{T}}$). One might think that this statement is only true for $\mathcal{O}(\kappa^2)$ and when one includes two-phonon processes [$\sim \mathcal{O}(\kappa^4)$], where the energy-momentum constraints can be relaxed, the decay rate of phonons will be a power law. In fact for scattering of a single massive particle by scalar fields, this is true, as shown in Refs. 70 and 71. However for a finite density of fermions, with a Fermi surface, it can be shown that for $T \ll c_s k$, the decay rate remains exponentially small ($\tau^{-1} \sim k e^{-\frac{c_s k}{T}}$) even when two-phonon processes are included in the description. This difference primarily arises from the fact that while the single particle can be treated classically ($\frac{p^2}{2m} \sim T$), the particle-hole excitations in our problem remain quantum objects as long as the phonons retain their quantum nature ($T \ll c_s k$). In the limit $T \gg c_s k$, we obtain $\tau^{-1} \sim T$. The difference in the exponent between our results and earlier works^{70,71} comes from considering the fact that the relevant two-phonon process is mediated by a fermion with energy mismatch (i.e. off-shell) $\sim (v_F - c_s)k$. Note that this is the dominant relaxation process for $(v_F - c_s)k \gg T \gg c_s k$, while the relaxation is dominated by the single phonon process for $T \sim (v_F - c_s)k$. See Appendix C for the detailed calculation. Note that two-phonon processes involve effectively one particle-hole excitation. Three-phonon processes, which involve two particle-

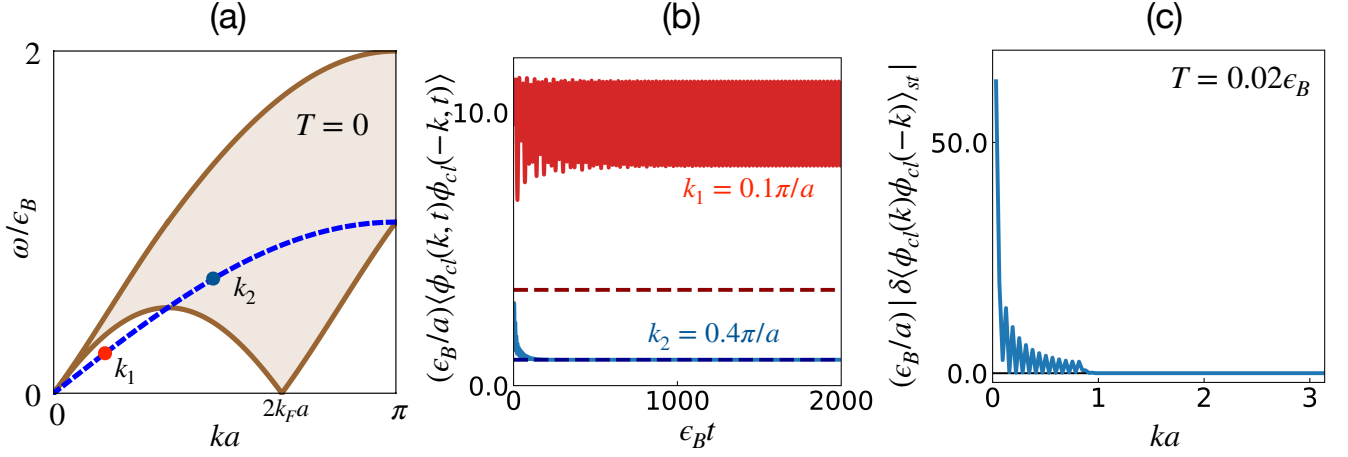


FIG. 2. Non-equilibrium dynamics of phonons coupled to a low temperature fermionic bath in one dimension. (a) The region of finite density of particle-hole excitations in the fermionic bath at $T = 0$ is shown in the $k - \omega$ plane as a shaded region. The solid brown lines define the upper and lower threshold energies. Note that the region collapses to a line (with slope v_F) at low momenta. The phonon dispersion for $c_s = \frac{1}{\sqrt{3}}v_F$ is also shown as a dashed line. The two momenta k_1 and k_2 , shown by the dots are chosen such that for k_1 , the phonon energy lies below the particle-hole bath while for k_2 , the energy lies within the bath. (b) Time evolution of the correlation function $iD^K(k; t, t) = \langle\phi_{cl}(k, t)\phi_{cl}(-k, t)\rangle$ for $k_1 = 0.1\pi/a$, where the phonons do not see a bath (red solid line) and for $k_2 = 0.4\pi/a$, where the phonons see an effective bath (solid blue line). k_1 and k_2 are shown in (a). The correlator at k_1 oscillates about its initial value and never approaches its thermal value shown by the dashed red line. On the other hand, the mode at k_2 is damped and the correlator approaches its thermal value (dashed blue line) at long times. We have used a bath with $T = 0.02\epsilon_B$ and $\mu = 0.5\epsilon_B$ and a system-bath coupling strength $\kappa^2 = 0.5\epsilon_B^3 a$. (c) The deviation of the long time value of the correlator from its thermal value plotted as a function of momenta. The long wavelength modes do not thermalize while the higher momentum correlators approach their thermal value. The value of the correlator for modes that do not thermalize depend on the initial conditions. The oscillations corresponds to the initial (1,0,1,0,1,0...) pattern of occupation of the momentum modes.

hole excitations also satisfy energy-momentum conservation constraints. They can result in a decay rate which is polynomial in temperature and hence not exponentially small. But these processes are of $\mathcal{O}(\kappa^8)$ and for small values of system-bath coupling they are highly suppressed.

To see this, we consider the case where the density of bath electrons gives $\mu = 0.5\epsilon_B$, so that $v_F = \frac{\sqrt{3}}{2}\epsilon_B a$. We choose a phonon dispersion with $\omega_0 = \epsilon_B$ so that $c_s = 0.5\epsilon_B a$, i.e. $c_s = \frac{1}{\sqrt{3}}v_F$. Here the phonon dispersion lies below the electronic dispersion at low momenta, as shown by the dashed line in Fig. 2(a). We consider a low bath temperature of $T = 0.02\epsilon_B$ to illustrate the low temperature behaviour of the system. We have set the system-bath coupling strength $\kappa^2 = 0.5\epsilon_B^3 a$. In Fig. 2(b), we plot the time dependence of the correlation function $iD^K(k; t, t) = \langle\phi_{cl}(k, t)\phi_{cl}(-k, t)\rangle$ for the setup given above (solid lines) for two different momenta: a low momentum $k_1 = 0.1\pi/a$, where the phonon dispersion is outside the energy range of the bath, and a high momentum $k_2 = 0.4\pi/a$, where the phonon dispersion lies within the bath energy range. The thermal value of the correlator is also indicated in this plot with dashed lines. It is clear that the mode at k_2 thermalizes, whereas the long wavelength mode k_1 does not thermalize in this case. The correlator at k_1 undergoes unitary quantum dynamics with a dressed phonon energy, oscillating about its initial value and never approaching the thermal value shown with the dashed red line.

On the other hand, the damped correlator at k_2 approaches the thermal value (dashed blue line) at long times. To see which modes are thermalizing, we plot the difference between the long-time value of the non-equilibrium correlators and its thermal value, $i\delta D^K(k; t, t) = \delta\langle\phi_{cl}(k, t)\phi_{cl}(-k, t)\rangle$, as a function of k in Fig. 2(c). We use the value of the correlator at $\epsilon_B t = 10^4$ as the “long time” value, and average over a timescale of $\epsilon_B t \sim 10^3$ to smooth out effects of the oscillations in modes that do not thermalize. It is clear that the low momentum modes that lie outside the effective bath do not thermalize. For these modes, the long time value of the correlator depends on the initial condition, and the oscillations with k represent the (1,0,1,0,1,0...) pattern of initial occupation.

The energy conservation constraints are relaxed as we increase the bath temperature. In this case, the bath spectral function gains weight at low energies starting from $\omega = 0$ for all k . The region in the $k - \omega$ plane where $J(k, \omega)$ is finite at high temperatures is shown as shaded region in Fig. 3(a). Note that the finite bandwidth of the fermions still results in an ultraviolet cut-off in the bath; i.e. for each k , there is a maximum energy $\omega_{max}(k) = 2\epsilon_B \sin(ka/2)$ beyond which the bath has no spectral weight at any temperature. This is plotted as a solid line in Fig. 3(a). One would thus expect the low momentum modes to thermalize once the bath has sufficiently high temperature, provided the phonon dispersion lies below this maximum energy, i.e. the phonon velocity $c_s < \epsilon_B a$, which is expected to be valid in generic one dimensional ma-

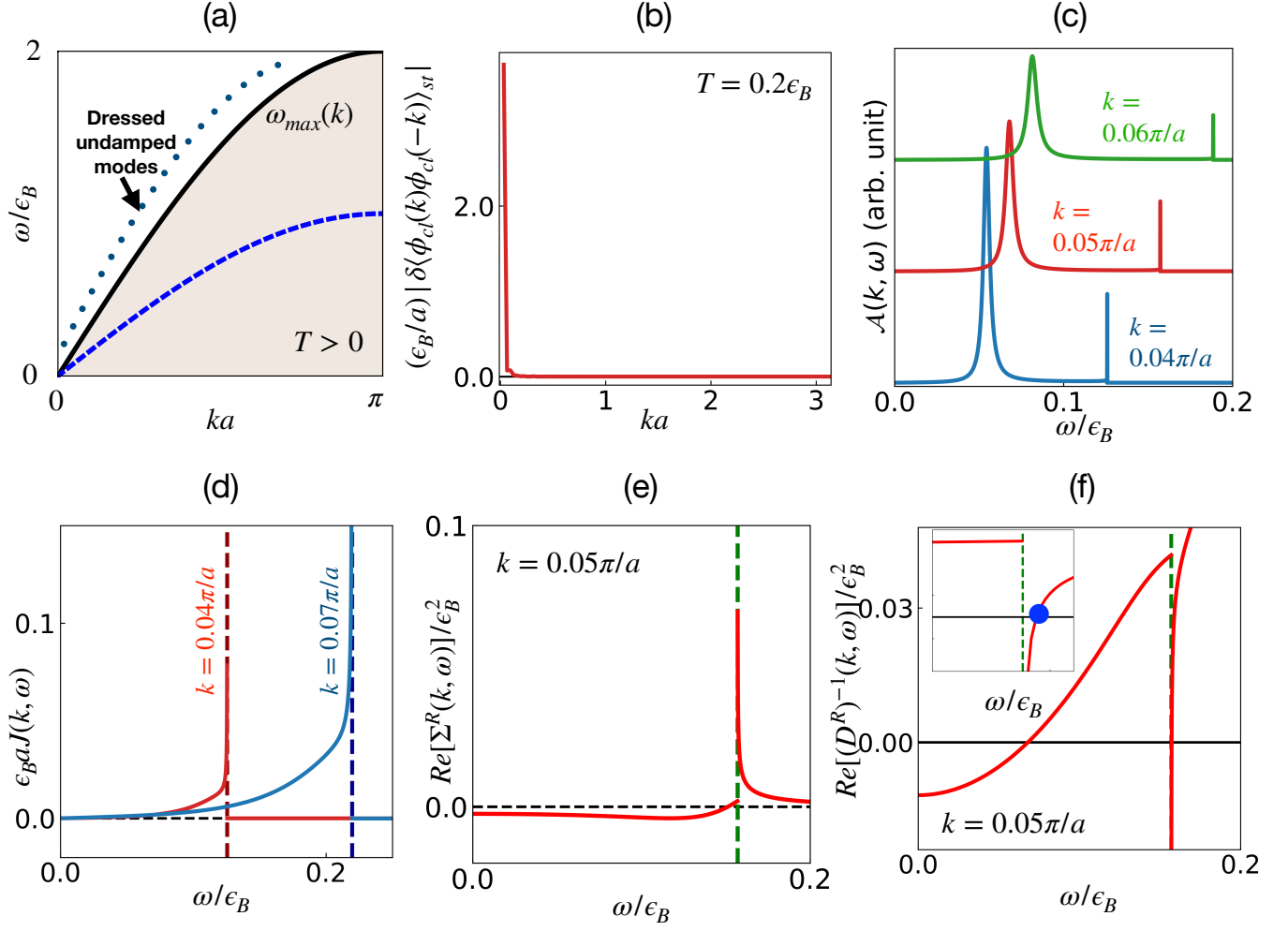


FIG. 3. Dynamics of phonons coupled to high temperature fermionic bath and emergence of dressed undamped modes in one dimension. (a) Particle-hole density of states (DOS) of the fermionic bath is finite only in the shaded region in the $k - \omega$ plane at finite temperature. It is bounded above by the solid black line given by $\omega_{max}(k) = 2\epsilon_B \sin(ka/2)$. The phonon dispersion with $c_s = 0.5\epsilon_B a$ is also plotted as a dashed blue line. The dots above $\omega_{max}(k)$ correspond to the undamped “polariton” modes formed due to strong fermion-phonon coupling. (b) The deviation of the correlation function at long times from its thermal value at a moderate temperature $T = 0.2\epsilon_B$ and system-bath coupling strength $\kappa^2 = 0.5\epsilon_B^3 a$. A few long wavelength phonon modes do not thermalize. (c) Phonon spectral function for a few low momentum modes. The broader peak represents the original dressed damped modes of the phonons. The sharp peaks indicate undamped modes. (d) Bath spectral functions for $k = 0.04\pi/a$ and $k = 0.07\pi/a$ are plotted in solid red and blue lines respectively. They have sharp cut-offs at $\omega = \omega_{max}(k)$, indicated by dashed vertical lines. The spectral function has a $\frac{1}{\omega_{max}(k) - \omega}$ singularity near this edge. (e) $\text{Re}[\Sigma^R(k, \omega)]/\epsilon_B^2$ as function of ω for $k = 0.05\pi$. It diverges at $\omega = \omega_{max}(k)$ (vertical green dashed line) from above and goes to a constant value inside. (f) The real part of the inverse propagator of phonon modes dressed by the fermionic bath. The inverse propagator has two zero crossings, one near the bare phonon frequency, corresponding to damped dressed phonons, and one above the bath edge ($\omega_{max}(k)$, shown as dashed green line) corresponding to undamped polaritons [inset shows the region near $\omega_{max}(k)$ clearly showing the second zero crossing].

terial systems like nanowires^{94,95}. In Fig. 3(b), we plot the difference between the long time value and the thermal value of the correlator, $i\delta D^K(k; t, t) = \delta\langle\phi_{cl}(k, t)\phi_{cl}(-k, t)\rangle$ for the phonon modes with $c_s = \frac{v_F}{\sqrt{3}}$, for which we had earlier looked at thermalization at low bath temperatures. The dispersion of this mode is shown as a dashed blue line in Fig. 3(a). We see that the low momentum modes do not thermalize even at a reasonably high temperature of $T = 0.2\epsilon_B$, although all the modes now see a particle-hole bath with sufficient spectral weight. We note that this lack of thermalization persists if the

temperature of the bath is further increased.

To get an insight into the lack of thermalization of low momentum modes even at high temperatures, in Fig. 3(c), we plot the spectral function of the dressed phonons in the steady state,

$$\mathcal{A}(k, \omega) = -(1/\pi)\text{Im}D^R(k, \omega), \quad (27)$$

as a function of ω for several values of k . In Fig. 3(c), the spectral functions for different modes are shifted by arbitrary

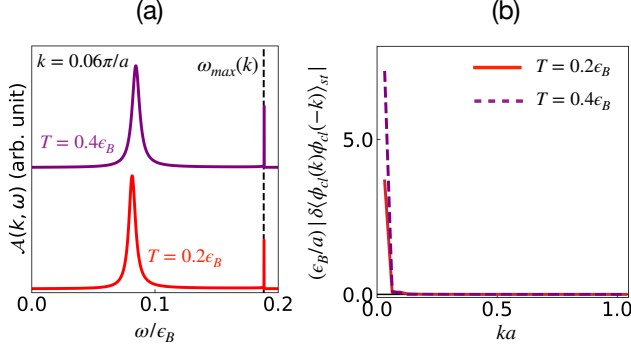


FIG. 4. Effect of temperature on non-thermalizing behaviour of phonon modes. (a) Phonon spectral function at $T = 0.2\epsilon_B$ and $T = 0.4\epsilon_B$ for the mode $k = 0.06\pi/a$ which does not thermalize. As temperature is increased, the polarinon mode remains sharp. (b) Absolute difference of the long time correlation function from its thermal value at long time for two temperatures $T = 0.2\epsilon_B$ (solid red line) and $T = 0.4\epsilon_B$ (dashed purple line). We notice finite deviation at low momenta at both the temperatures. The system-bath coupling strength is $\kappa^2 = 0.5\epsilon_B^3 a$.

amounts to make them visible. In addition to the original phonon mode, which is dressed and has a width, we find another sharp mode with no damping at an energy above the boundary of the particle-hole bath. This mode appears due to the strong coupling between the phonons and the electron-hole pairs, similar to polariton modes which occur due to strong coupling between photons and excitons^{72,73}. We will call these modes the “polarinon” modes. A key difference with polaritons is that unlike excitons, the particle-hole excitations are not coherent; i.e. a simple mode coupling theory would not work here. Rather the origin of this mode can be traced back to the strong $\sim 1/\sqrt{\omega_{max}(k) - \omega}$ divergence of the spectral density of the particle-hole excitations at the band edge in 1-d, which gives a similar divergence in $\text{Im}\Sigma^R(k, \omega)$. This is shown in Fig. 3(d), where we plot the bath spectral function for two different values of k at $T = 0.2\epsilon_B$ and $\mu = 0.5\epsilon_B$. Using Kramers-Kronig relations⁹⁶, one can easily show that this would also lead to a $\sim 1/\sqrt{\omega - \omega_{max}(k)}$ divergence in $\text{Re}\Sigma^R(k, \omega)$ for frequencies just above the band edge. This is shown in Fig. 3(e), where it is evident that $\text{Re}\Sigma^R(k, \omega) \rightarrow +\infty$ as we approach the band edge from above. In contrast, the real part of the self energy approaches a constant as the frequency comes close to the band edge from below. The real part of the retarded self energy dresses the spectrum, and its divergence ensures that $D^{R-1}(k, \omega) = 2(\omega^2 - \Omega_k^2) - \Sigma^R(k, \omega)$ has zeroes just above the upper edge of the bath; i.e. close to $\omega \sim \omega_{max}(k)$. This is shown in Fig. 3(f), where $\text{Re} D^{R-1}(k, \omega)$ is plotted as a function of ω , revealing the two zero crossings. The lower energy zero crossing is related to the phonon mode (now dressed by the bath), while the higher frequency zero crossing (shown more clearly in the inset) is related to divergence of the bath spectral function. Thus the strong divergence of the bath density of states leads to an additional pole in the dressed phonon

Green’s function above the upper edge of the bath. This undamped “polarinon” mode, which shows up as a sharp feature in Fig. 3(c), does not thermalize even at high temperatures. This explains the lack of thermalization seen in Fig. 3(b) even for high temperatures where the bare phonon sees a substantial bath spectral density.

The dispersion of the polarinon mode ω_k^{pl} is shown schematically as a dotted line in Fig. 3(a). We note that the quasiparticle residue for the polarinon is given by (see Appendix D for details)

$$Z^{pl}(k) = \left[4\omega_k^{pl} - \frac{\partial \text{Re}\Sigma^R(k, \omega)}{\partial \omega} \Big|_{\omega_k^{pl}} \right]^{-1} \sim \frac{[\omega_k^{pl} - \omega_{max}(k)]^{\frac{3}{2}}}{[\lambda(k)]^2} \quad (28)$$

As k increases, $\omega_k^{pl} - \omega_{max}(k)$ increases, while $1/[\lambda(k)]^2$ decreases. The suppression from the form factor dominates over the increase in separation between the polarinon energy and the band edge, and the quasiparticle residue of this mode decreases with increasing k . Thus the polarinon dominated lack of thermalization is not seen at large momenta. Further, since the polarinon occurs outside the band edge it is not smeared out by thermal fluctuations. This is shown in Fig. 4(a), where we plot the spectral function of a phonon mode with $k = 0.06\pi/a$ at two different temperatures, $T_1 = 0.2\epsilon_B$ and $T_2 = 0.4\epsilon_B$. While the original phonon mode broadens with increasing temperature, the polarinon mode remains sharp with almost constant spectral weight at these two temperatures. With increasing temperature, the deviations of the phonon correlators from their thermal values increases slightly, as seen in Fig. 4(b).

To summarize, in one dimension, phonons coupled to fermionic baths do not thermalize, especially the modes at low momenta. At low temperature, this is primarily due to strong energy momentum constraints, which leads to a very narrow energy band of particle-hole excitations at low momenta. However, the lack of thermalization at high temperatures is dominated by the formation of undamped polarinon modes with energies above the bath band edge due to strong divergence of the bath density of states near the band edge. The effect of these modes increases with electron-phonon coupling in the system. The effect also increases if the phonons are stiffer, so that the gap between the phonon dispersion and the band edge is reduced.

2. Two dimensional systems

In this section, we will consider the non-equilibrium dynamics of phonons coupled to fermions in two dimensions and see how the dynamics differs from that in one dimension. As we have seen before, the dynamics is governed by the density of states of particle-hole pairs of fermions. Contrary to one dimension, the energy momentum conservation relations can be satisfied much more easily in two dimensions. Hence even at $T = 0$, the density of states of particle-hole excitations with a given momentum transfer k remains finite at arbitrary low energies. The finite band-

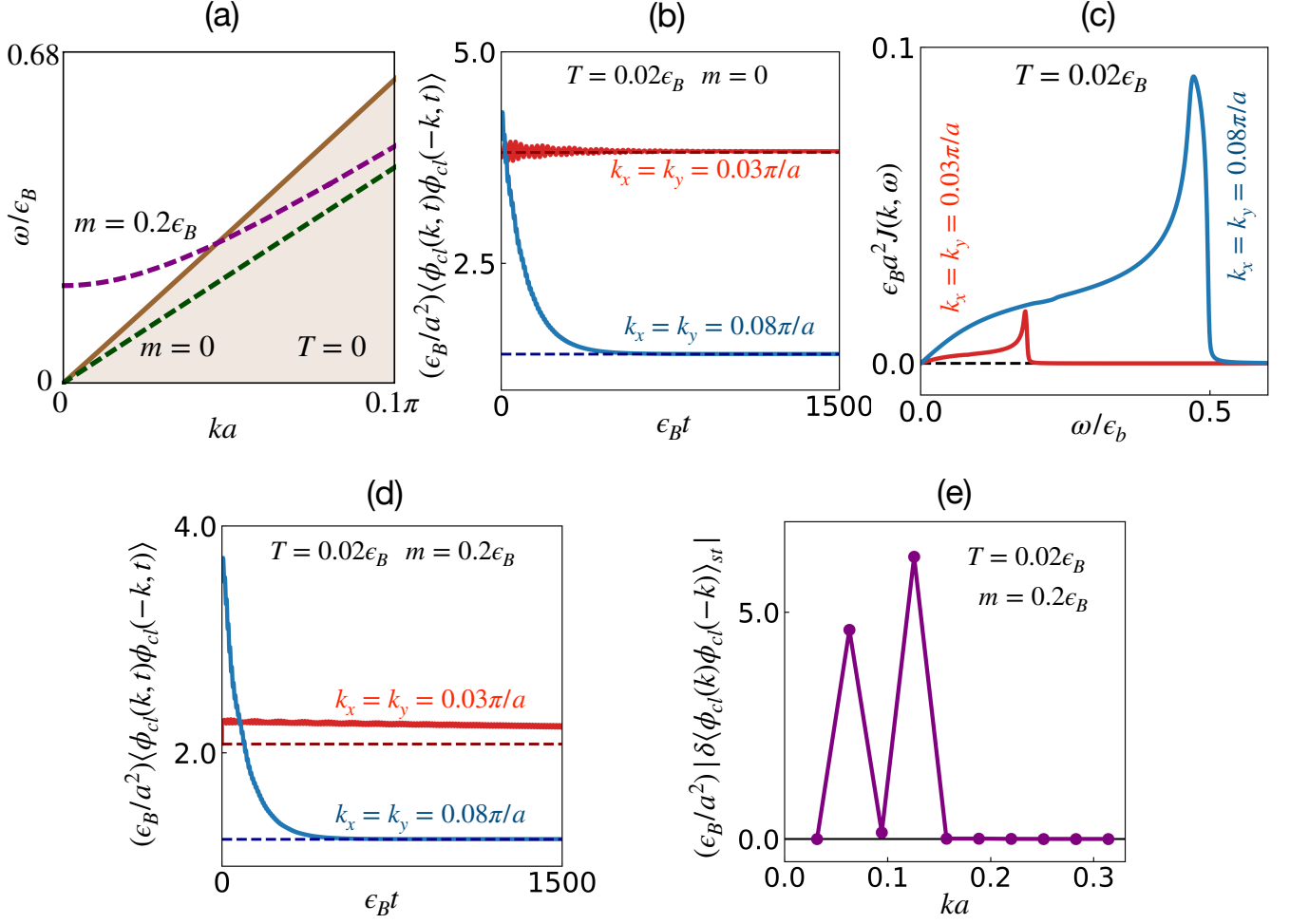


FIG. 5. Non-equilibrium dynamics of phonons coupled to fermionic bath in two dimensions. (a) A schematic depiction of particle-hole density of states (DOS) of the fermionic bath on $\mathbf{k} - \omega$ plane along $(1, 1)$ direction where $\mathbf{k} = (k, k)$ at $T = 0$. The shaded region, from $\omega = 0$ to $\omega_{max}(\mathbf{k}) = \frac{\sqrt{2}v_F}{a} \sin ka + \mu(1 - \cos ka)$ (shown in brown solid line) has finite DOS. The dispersion of acoustic (massless) phonons ($m = 0$) with $c_s = \epsilon_B a = 0.73v_F$ is given by the dashed green line. The dashed purple line is the dispersion of optical (massive) phonons with $m = 0.2\epsilon_B$ and $c_s = \epsilon_B a = 0.73v_F$. (b) Time evolution of the correlation function $iD^K(\mathbf{k}; t, t) = \langle \phi_{cl}(\mathbf{k}, t) \phi_{cl}(-\mathbf{k}, t) \rangle$ at $\mathbf{k} = (0.03\pi/a, 0.03\pi/a)$ (red solid line) and $\mathbf{k} = (0.08\pi/a, 0.08\pi/a)$ (blue solid line) for massless phonons are plotted. Both the correlators relax to their thermal values (shown with dashed lines) at long times. (c) Bath spectral functions for $\mathbf{k} = (0.03\pi/a, 0.03\pi/a)$ and $\mathbf{k} = (0.08\pi/a, 0.08\pi/a)$ are plotted in solid red and blue lines respectively. Their finite value at low ω indicates the absence of a lower bound in two dimensions. Unlike in one dimension, there is no divergence in the bath spectral function in two dimensions. (d) Dynamics of the correlation function $iD^K(\mathbf{k}; t, t)$ at $\mathbf{k} = (0.03\pi/a, 0.03\pi/a)$ (red line) and $\mathbf{k} = (0.08\pi/a, 0.08\pi/a)$ (blue line) for massive phonons with $m = 0.2\epsilon_B$ and $c_s = \epsilon_B a = 0.73v_F$. The dispersion of the mode at $\mathbf{k} = (0.03\pi/a, 0.03\pi/a)$ lies above the band threshold and hence the correlator does not relax to its thermal value (shown by dashed red line). On the other hand, the energy of the mode at $\mathbf{k} = (0.08\pi/a, 0.08\pi/a)$ lies within the region of finite bath spectral function. So the corresponding correlator relaxes to its thermal value at long times. (e) The deviation of the long time value of the correlation function $iD^K(\mathbf{k}; t, t)$ from its thermal value as a function of momenta. The low momentum modes, with dispersion above the band threshold do not thermalize. All data in this figure are obtained for a bath temperature $T = 0.02\epsilon_B$ and chemical potential $\mu = 0.5\epsilon_B$ and system-bath coupling strength $\kappa^2 = 0.5\epsilon_B^3 a^2$.

width of the lattice fermions leads to an upper threshold energy $\omega_{max}(\mathbf{k}) = \frac{\sqrt{2}v_F}{a} \sin ka + \mu(1 - \cos ka)$ along the $(1, 1)$ direction where $\mathbf{k} = (k, k)$. It disperses linearly at low $|\mathbf{k}|$, i.e. $\omega_{max}(\mathbf{k}) \sim v_F k$, where v_F is the Fermi velocity of the fermions in the bath. Beyond this threshold energy the density of states of particle-hole excitations vanish. In Fig. 5(a) the particle-hole DOS is sketched schematically

in the $\mathbf{k} - \omega$ plane along the $(1, 1)$ direction in \mathbf{k} -space up to $\mathbf{k} = (0.1\pi/a, 0.1\pi/a)$. In the figure, the upper bound $\omega_{max}(\mathbf{k})$ is represented by a solid brown line. In the shaded region below this line we have finite particle-hole DOS.

Linearly dispersing long wavelength phonon modes with $c_s < v_F$ would see a bath with substantial spectral density even at very low temperatures and would thermalize. In

Fig. 5(a), we also plot the bare dispersion of a longitudinal phonon mode with $c_s = 0.73v_F$ as a green dashed line to illustrate this point. Note that the criterion $c_s < v_F$ is satisfied for most material systems other than compensated semimetals⁹⁷⁻⁹⁹ or bilayer graphene¹⁰⁰ near its charge neutrality point. In these systems, by tuning the carrier density, one can possibly see a lack of thermalization of the phonons, although at these very low densities, disorder and interaction would play a very important role^{101,102} and the simple picture of a non-interacting bath has to be suitably modified. In Fig. 5(b) we have plotted the dynamics of the correlation function $\langle \phi_{cl}(\mathbf{k}, t) \phi_{cl}(-\mathbf{k}, t) \rangle$ as a function of time for massless phonon modes ($c_s = 0.73v_F$) with two different values of momenta, $\mathbf{k}_1 = (0.03\pi, 0.03\pi)$ (red line) and $\mathbf{k}_2 = (0.08\pi, 0.08\pi)$ (blue line) at a low temperature $T = 0.02\epsilon_B$ and system-bath coupling strength $\kappa^2 = 0.5\epsilon_B^3 a^2$. The thermal values of the correlators are indicated by the dashed lines. It is clear in this case that both these modes thermalize at long times.

We would like to note that the bath density of states in two dimensions do not have the strong divergence at the band edges that was present in the one dimensional case. This is shown in Fig. 5(c), where we plot the spectral density of the particle-hole excitations for two different momentum transfers. The softening of the band edge non-analyticity means that there is no corresponding divergence in the real part of self energy and hence there are no additional undamped dressed states (poles in the Green's function) of the system. Thus the system continues to thermalize as temperature is increased, unlike the one dimensional phonons.

The thermalization of the scalar fields can be prohibited if the fields are massive. In the context of phonons, this would correspond to optical phonons in the system¹⁰³. The low momentum dispersion of the massive fields, with $m = 0.2\epsilon_B$ is plotted in Fig. 5(a) as a dashed purple line. As $k \rightarrow 0$, the dispersion of the phonons lies above the bandwidth of the particle-hole excitations and hence one would expect that the long wavelength modes would not thermalize. As the momentum is increased, the dispersion enters the region of finite bath spectral density and these higher momentum modes thermalize. This is clearly seen in Fig. 5(d) where we plot the time evolution of the correlator $\langle \phi_{cl}(\mathbf{k}, t) \phi_{cl}(-\mathbf{k}, t) \rangle$ (solid lines) for two different values of \mathbf{k} along with the thermal values of the correlators (dashed lines). The mode with the low momentum $(0.03\pi/a, 0.03\pi/a)$ (shown by red line) does not thermalize as its energy lies above the bath band. It oscillates about its initial value sufficiently far from the thermal value (dashed red line). On the other hand, the correlator of the mode at $(0.08\pi/a, 0.08\pi/a)$, which lies within the bath energy ranges, approaches its thermal value in the long time limit. Fig. 5(e) plots the deviation of the long time correlation functions from their thermal value as a function of $|\mathbf{k}|/\sqrt{2}$ along the $(1, 1)$ direction. It is clear that there is a sharp cut-off in momentum, below which the modes do not thermalize for the massive scalar field. This corresponds to the lowest momentum for which the dressed dispersion lies below $\omega_{max}(\mathbf{k})$.

IV. CONCLUSION

In this paper, we have proposed a new method to study non-equilibrium dynamics of scalar fields starting from non-thermal initial conditions. This extends earlier work on Schrödinger bosons⁵¹ to the case of scalar fields. The method works by adding a source to the bilinears of quantum fields at the initial time in a Schwinger-Keldysh field theoretic formalism. The correlation functions are calculated in presence of this source. One then takes a set of derivatives of this correlation function with respect to this source (with the set determined by the initial conditions) to obtain the physical correlators. The key difference between the earlier and present formalism is the coupling of the sources to both the fields and their time derivatives, reflecting the nature of the classical equations of motion.

We use this method to study non-equilibrium dynamics of massless and massive scalar fields, initialized to athermal states, and coupled to external baths. For concreteness, we consider a system of phonons with the massive fields corresponding to optical phonons and the massless fields corresponding to longitudinal phonons. We first consider coupling the system to an ohmic bath with a smooth ultraviolet cut-off. In this case, the system thermalizes with the one particle distributions relaxing to their thermal values. The relaxation rate is momentum dependent when the ultraviolet cut-off is small, and approaches a momentum independent Gaussian white noise limit as the cut-off is increased.

We then consider the dynamics of these phonon modes coupled to a system of non-interacting fermions, where the phonons couple to the particle-hole excitations of the system. In one dimension we find that the long wavelength phonons fail to thermalize at all temperatures. At low temperatures, this is due to the effectively zero bandwidth of the particle-hole excitations with small momentum transfer, as a result of which the long wavelength phonon modes do not see any bath and undergoes unitary quantum motion. At high temperatures, the lack of thermalization is dominated by the formation of undamped dressed modes just above the upper threshold of the bath. These modes are neither phonon, nor fermion modes; rather these ‘‘polarinon’’ modes arise due to strong fermion phonon coupling in the system together with divergences in the density of states of one dimensional particle-hole excitations. These modes remain sharp with increasing temperature; as a result the long wavelength modes fail to thermalize at any temperature.

We finally consider phonons coupled to fermionic baths in two dimensions. Here simultaneous energy momentum conservation does not lead to stringent criteria and the bath bandwidth is finite at low momenta at all temperatures. Further the strong divergence of density of states is also absent. As a result, we recover the typical thermalizing behaviour of the phonon modes in two dimensions.

We note that the method we have constructed is much more widely applicable than the models we have considered in this paper, including the study of non equilibrium dynamics of interacting scalar field theories. We believe this method will find much wider applications in the future.

ACKNOWLEDGMENTS

The authors are grateful to Ahana Chakraborty for useful discussions and suggestions. The authors acknowledge the

use of computational facilities at the Department of Theoretical Physics, Tata Institute of Fundamental Research, Mumbai for this paper. The authors acknowledge support of the Department of Atomic Energy, Government of India, under Project Identification No. RTI 4002.

Appendix A: Green's functions for single Harmonic Oscillator

In developing the extended Keldysh formalism for the harmonic oscillators in the position basis, a crucial step was the inversion of the matrix that appears in the u dependent action, Eq. (6). This leads to the u dependent one-particle correlator $D(u)$, which finally leads to the physical correlation functions in the system. In this appendix, we present the details of this non-trivial inversion.

The matrix in Eq. (6) can be separated two parts, one of which is independent of the source u . This decomposition can be written as

$$D^{-1}(t, t'; u) = D^{-1}(t, t'; 0) - \Delta(t, t'; u), \quad (\text{A1})$$

where

$$D^{-1}(t, t'; 0) = \delta(t - t') \begin{bmatrix} (-\partial_t^2 - \Omega^2) + \delta_{t0}(-\partial_t + i\omega) & 0 \\ 0 & (\partial_t^2 + \Omega^2) + \delta_{t0}(\partial_t + i\omega) \end{bmatrix}, \quad (\text{A2})$$

and

$$\Delta(t, t'; u) = i\omega \frac{2u}{1-u^2} [-u\mathbb{I}_2 + \sigma^x] \delta_{t0} \delta_{t'0}. \quad (\text{A3})$$

Here \mathbb{I}_2 is 2×2 identity matrix. Inverting $D^{-1}(t, t'; 0)$ we get the components of $D(t, t'; 0)$

$$\begin{aligned} D^{+-}(t, t', 0) &= \frac{1}{2\Omega} \sin \Omega(t - t') - \frac{i}{2\omega} \left\{ \cos \Omega t \cos \Omega t' + \frac{\omega^2}{\Omega^2} \sin \Omega t \sin \Omega t' \right\} \\ D^{-+}(t, t', 0) &= -\frac{1}{2\Omega} \sin \Omega(t - t') - \frac{i}{2\omega} \left\{ \cos \Omega t \cos \Omega t' + \frac{\omega^2}{\Omega^2} \sin \Omega t \sin \Omega t' \right\} \\ D^{++}(t, t', 0) &= \Theta(t - t') D^{-+}(t, t', 0) + \Theta(t' - t) D^{+-}(t, t', 0) \text{ and} \\ D^{--}(t, t', 0) &= \Theta(t - t') D^{+-}(t, t', 0) + \Theta(t' - t) D^{-+}(t, t', 0). \end{aligned} \quad (\text{A4})$$

One can easily check that $D^{-1}(t, t''; 0)D(t'', t'; 0) = \delta(t - t')\mathbb{I}_2$. Now $D(t, t'; u)$ can be found using the Dyson series

$$D(t, t'; u) = D(t, t'; 0) + D(t, 0; 0)[\Delta(0, 0; u) + \Delta(0, 0; u)D(0, 0; 0)\Delta(0, 0; u) + \dots]D(0, t'; 0) \quad (\text{A5})$$

Using the fact that $D(0, 0; 0) = \frac{i}{2\omega} [\mathbb{I} + \sigma^x]$, the series inside the brackets of Eq. (A5) can be evaluated using standard Pauli matrix identities to be $i\omega \left(\frac{2u}{1-u} \right) \sigma^x$. Using this and Eq. (A4) we get the source dependent Green's functions in Eq. (8). One then takes the required u derivatives to get the physical correlation function.

Appendix B: Phonon self energy from the fermionic bath

In this appendix we present the details of the derivation of the phonon self-energy when the phonons are coupled to a bath of free fermions through the Hamiltonian

$$H_{int} = \kappa \sum_{\mathbf{k}, \mathbf{q}} \lambda(\mathbf{k}) \psi^\dagger(\mathbf{k} + \mathbf{q}, t) \psi(\mathbf{q}, t) \phi(\mathbf{k}, t), \quad (\text{B1})$$

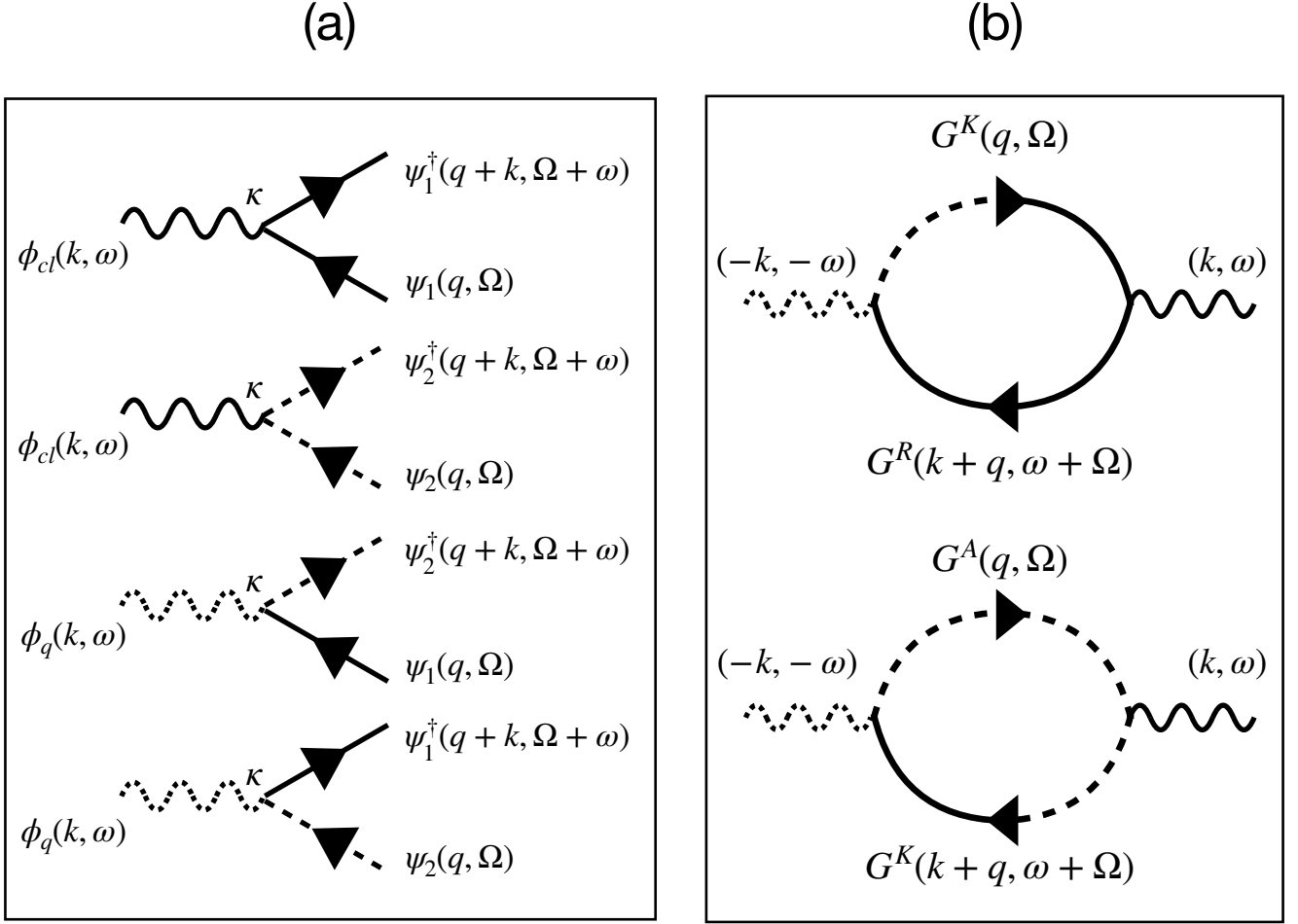


FIG. 6. Dressing of the phonons coupled to a fermionic bath. (a) Allowed interaction vertices in terms of the Keldysh rotated fields. The solid line represents the fermionic field ψ_1 (ψ_1^\dagger) and the dashed line represents ψ_2 (ψ_2^\dagger). Solid wavy line represents the scalar field ϕ_{cl} and the dotted wavy line stands for the scalar field ϕ_q . κ is the coupling strength between the scalar field and the fermions. (b) Diagrams for retarded self energy $\Sigma^R(\mathbf{k}, \omega)$ of phonons coupled to a fermionic bath. Note that the retarded self energy of phonons is related to the polarization function of the fermions. Note that the diagrammatic representations for G^R , G^A , G^K look different for bosons and fermions, since the Keldysh rotation is different, e.g. for fermions $G^K = i\langle\psi_1\psi_2^\dagger\rangle$ is represented by a dashed-solid line, while for bosons $G^K = i\langle\phi_{cl}\phi_{cl}\rangle$ would be represented by a solid-solid line.

where κ is the system bath coupling strength and $\lambda(\mathbf{k}) = \sqrt{\sum_{j=1}^D \sin^2(k_j a/2)}$ is related to the deformation potential acting between electrons and phonons⁹². On the Keldysh contour⁴⁹ (+/- basis) its contribution to the action is given by

$$S_{int} = -\kappa \sum_{\mathbf{k}, \mathbf{q}} \lambda(\mathbf{k}) \int_{-\infty}^{+\infty} dt \left[\psi_+^\dagger(\mathbf{k} + \mathbf{q}, t) \psi_+(\mathbf{q}, t) \phi_+(\mathbf{k}, t) - \psi_-^\dagger(\mathbf{k} + \mathbf{q}, t) \psi_-(\mathbf{q}, t) \phi_-(\mathbf{k}, t) \right] \quad (\text{B2})$$

It is useful to work in the Keldysh rotated basis⁴⁹. The Keldysh rotated basis for scalar fields are given by

$$\begin{aligned} \phi_{cl}(\mathbf{k}, t) &= \frac{1}{2} [\phi_+(\mathbf{k}, t) + \phi_-(\mathbf{k}, t)] \\ \phi_q(\mathbf{k}, t) &= \frac{1}{2} [\phi_+(\mathbf{k}, t) - \phi_-(\mathbf{k}, t)], \end{aligned} \quad (\text{B3})$$

while Keldysh rotated basis for fermions is given by

$$\begin{aligned}\psi_1(\mathbf{k}, t) &= \frac{1}{\sqrt{2}}[\psi_+(\mathbf{k}, t) + \psi_-(\mathbf{k}, t)] & \psi_2(\mathbf{k}, t) &= \frac{1}{\sqrt{2}}[\psi_+(\mathbf{k}, t) - \psi_-(\mathbf{k}, t)] \\ \psi_1^\dagger(\mathbf{k}, t) &= \frac{1}{\sqrt{2}}[\psi_+^\dagger(\mathbf{k}, t) - \psi_-^\dagger(\mathbf{k}, t)] & \psi_2^\dagger(\mathbf{k}, t) &= \frac{1}{\sqrt{2}}[\psi_+^\dagger(\mathbf{k}, t) + \psi_-^\dagger(\mathbf{k}, t)].\end{aligned}\quad (\text{B4})$$

In the Keldysh rotated basis the fermion-phonon coupling can be written as

$$\begin{aligned}S_{int} &= -\kappa \sum_{\mathbf{k}, \mathbf{q}} \lambda(\mathbf{k}) \int_{-\infty}^{+\infty} dt [\psi_1^\dagger(\mathbf{k} + \mathbf{q}, t) \psi_1(\mathbf{q}, t) \phi_{cl}(\mathbf{k}, t) + \psi_2^\dagger(\mathbf{k} + \mathbf{q}, t) \psi_2(\mathbf{q}, t) \phi_{cl}(\mathbf{k}, t) \\ &\quad + \psi_1^\dagger(\mathbf{k} + \mathbf{q}, t) \psi_2(\mathbf{q}, t) \phi_q(\mathbf{k}, t) + \psi_2^\dagger(\mathbf{k} + \mathbf{q}, t) \psi_1(\mathbf{q}, t) \phi_q(\mathbf{k}, t)].\end{aligned}\quad (\text{B5})$$

In frequency space it turns into

$$\begin{aligned}S_{int} &= -\kappa \sum_{\mathbf{k}, \mathbf{q}} \lambda(\mathbf{k}) \int_{-\infty}^{+\infty} \frac{d\omega}{2\pi} \int_{-\infty}^{+\infty} \frac{d\Omega}{2\pi} [\psi_1^\dagger(\mathbf{k} + \mathbf{q}, \omega + \Omega) \psi_1(\mathbf{q}, \Omega) \phi_{cl}(\mathbf{k}, \omega) + \psi_2^\dagger(\mathbf{k} + \mathbf{q}, \omega + \Omega) \psi_2(\mathbf{q}, \Omega) \phi_{cl}(\mathbf{k}, \omega) \\ &\quad + \psi_1^\dagger(\mathbf{k} + \mathbf{q}, \omega + \Omega) \psi_2(\mathbf{q}, \Omega) \phi_q(\mathbf{k}, \omega) + \psi_2^\dagger(\mathbf{k} + \mathbf{q}, \omega + \Omega) \psi_1(\mathbf{q}, \Omega) \phi_q(\mathbf{k}, \omega)].\end{aligned}\quad (\text{B6})$$

The terms in Eq. (B6) gives allowed vertices for system-bath coupling. They are sketched in Fig. 6(a). Diagrams for retarded self energy of the phonons are sketched in Fig. 6(b), where solid straight lines represent $\psi_1(\psi_1^\dagger)$, dashed straight lines represent $\psi_2(\psi_2^\dagger)$, solid wavy lines indicate ϕ_{cl} and dashed wavy lines represent ϕ_q . Note that due to different Keldysh rotations for fermionic and bosonic fields (we follow the convention in Ref. 49), the diagrammatic representations of the bosonic and fermionic propagators look different, e.g. while $G^K = i\langle\phi_{cl}\phi_{cl}\rangle$ for bosons is represented by a fully solid line, for fermions $G^K = i\langle\psi_1\psi_2^\dagger\rangle$ is represented by a dashed-solid line. Similar adjustments occur for G^R and G^A as well. The diagrams for self-energy are given in terms of the vertices and free fermionic Green's functions. The retarded self energy is

$$\Sigma^R(\mathbf{k}, \omega) = -i\kappa^2 \lambda(\mathbf{k})^2 \sum_{\mathbf{q}} \int_{-\infty}^{\infty} \frac{d\Omega}{2\pi} [G^R(\mathbf{k} + \mathbf{q}, \omega + \Omega) G^K(\mathbf{q}, \Omega) + G^K(\mathbf{k} + \mathbf{q}, \omega + \Omega) G^A(\mathbf{q}, \Omega)].\quad (\text{B7})$$

Here Green's functions of the free fermions at thermal equilibrium are

$$G_0^R(\mathbf{k}, \omega) = [G^A(\mathbf{k}, \omega)]^* = \frac{1}{\omega - \epsilon_{\mathbf{k}} + i0^+} \quad \text{and} \quad (\text{B8})$$

$$G_0^K(\mathbf{k}, \omega) = -2\pi i F(\omega) \delta(\omega - \epsilon_{\mathbf{k}}), \quad (\text{B9})$$

where $F(\omega) = \tanh\left(\frac{\omega - \mu}{2T}\right)$. T is the temperature of the bath and μ is the chemical potential.

It is then easy to see (see Fig. 6(b) for the corresponding Feynman diagrams) that the retarded self energy for phonons is just the polarization function of free Fermi gas multiplied by factors of system-bath coupling strength. Upon simplifying we get,

$$\begin{aligned}\Sigma^R(\mathbf{k}, \omega) &= \kappa^2 \lambda(\mathbf{k})^2 \sum_{\mathbf{q}} \frac{F(\epsilon_{\mathbf{k}+\mathbf{q}}) - F(\epsilon_{\mathbf{q}})}{\omega + i0^+ + \epsilon_{\mathbf{q}} - \epsilon_{\mathbf{k}+\mathbf{q}}} \\ &= -\kappa^2 \lambda(\mathbf{k})^2 \int_{-\infty}^{\infty} \frac{d\omega'}{2\pi} \frac{J(\mathbf{k}, \omega')}{\omega' - \omega - i0^+},\end{aligned}\quad (\text{B10})$$

where bath spectral function $J(k, \omega)$ is given by

$$J(\mathbf{k}, \omega) = \pi \lambda(\mathbf{k})^2 \sum_{\mathbf{q}} [F(\epsilon_{\mathbf{k}+\mathbf{q}}) - F(\epsilon_{\mathbf{q}})] \delta(\omega - \epsilon_{\mathbf{k}+\mathbf{q}} + \epsilon_{\mathbf{q}}). \quad (\text{B11})$$

The Keldysh self energy is given by (using fluctuation-dissipation theorem)

$$\begin{aligned}
\Sigma^K(\mathbf{k}, \omega) &= 2i \coth\left(\frac{\omega}{2T}\right) \text{Im}[\Sigma^R(\mathbf{k}, \omega)] \\
&= -i2\pi\kappa^2 \lambda(\mathbf{k})^2 \sum_{\mathbf{q}} \coth\left(\frac{\omega}{2T}\right) [F(\epsilon_{\mathbf{k}+\mathbf{q}}) - F(\epsilon_{\mathbf{q}})] \delta(\omega - \epsilon_{\mathbf{k}+\mathbf{q}} + \epsilon_{\mathbf{q}}) \\
&= -i2\pi\kappa^2 \lambda(\mathbf{k})^2 \sum_{\mathbf{q}} \coth\left(\frac{\epsilon_{\mathbf{k}+\mathbf{q}} - \mu}{2T} - \frac{\epsilon_{\mathbf{q}} - \mu}{2T}\right) \left[\tanh\left(\frac{\epsilon_{\mathbf{k}+\mathbf{q}} - \mu}{2T}\right) - \tanh\left(\frac{\epsilon_{\mathbf{q}} - \mu}{2T}\right) \right] \delta(\omega - \epsilon_{\mathbf{k}+\mathbf{q}} + \epsilon_{\mathbf{q}}) \\
&= -i2\pi\kappa^2 \lambda(\mathbf{k})^2 \sum_{\mathbf{q}} \left[1 - \tanh\left(\frac{\epsilon_{\mathbf{k}+\mathbf{q}} - \mu}{2T}\right) \tanh\left(\frac{\epsilon_{\mathbf{q}} - \mu}{2T}\right) \right] \delta(\omega - \epsilon_{\mathbf{k}+\mathbf{q}} + \epsilon_{\mathbf{q}}) \\
&= i2\pi\kappa^2 \lambda(\mathbf{k})^2 \sum_{\mathbf{q}} [F(\epsilon_{\mathbf{k}+\mathbf{q}}) F(\epsilon_{\mathbf{q}}) - 1] \delta(\omega - \epsilon_{\mathbf{k}+\mathbf{q}} + \epsilon_{\mathbf{q}}).
\end{aligned} \tag{B12}$$

Appendix C: Multi-phonon processes and phonon relaxation

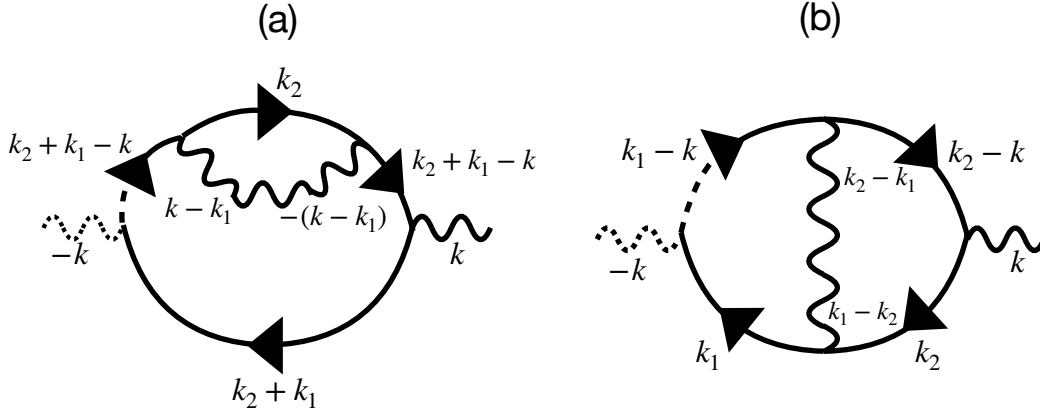


FIG. 7. Multi-phonon processes giving rise to $\mathcal{O}(\kappa^4)$ corrections to the phonon self energy: (a) A representative diagram where the fermion correlators in the polarization function are dressed by self energy corrections due to emission/absorption of an additional phonon. Note that the particle-hole pair with momenta $(k_1 + k_2, k_2)$ together with the phonon at $k - k_1$ can satisfy the energy-momentum conservation criterion. The intermediate fermion lines at $k_2 + k_1 - k$ are off-shell propagators. There are many such diagrams for the retarded self energy. We have shown one to indicate the structure of the diagram. (b) A representative diagram where the polarization function of the fermions is dressed by a vertex. These vertex corrections do not play leading role in relaxing the energy momentum constraints and are neglected in our calculations. Once again we have shown one of the many vertex diagrams to illustrate their structure.

We have shown in the main text that the energy momentum constraints in 1D lead to an exponentially small relaxation rate for the phonons at low temperatures. We have shown this to $\mathcal{O}(\kappa^2)$, where the phonon self energy is proportional to the polarization function of the fermionic bath. A natural question arises: Do multi-phonon processes, where other phonons can carry away energy and momentum, relax the constraints and lead to a power law behaviour at low T ? Earlier works, which modelled relaxation of a single particle in a Luttinger liquid⁷⁰ or in spinor gas⁷¹, predicted a scattering rate $\Gamma \sim T^4$, coming from two-phonon processes. In this appendix we show that for our problem of phonons coupled to a Fermi sea, the scattering rate remains exponentially small at low $T \ll c_s k$; i.e. $\Gamma_k \sim k e^{-c_s k/T}$. For $T \gg c_s k$, we recover the expected thermal broadening $\Gamma_k \sim T$. The key difference between our paper and earlier works stems from the fact that we are considering a finite density of particles with a Fermi sea whereas the earlier works^{70,71} considered a single particle.

We would like to note that since we are interested in the decay rate for phonons, we focus on the imaginary part of the retarded self-energy of the phonons on shell, i.e.

$$\Gamma_k \sim -\frac{1}{\Omega_k} \text{Im} \Sigma_{(4)}^R(k, \Omega_k), \tag{C1}$$

calculated to $\mathcal{O}(\kappa^4)$. There are two types of diagrams which contribute at $\mathcal{O}(\kappa^4)$: (i) diagrams where the fermion lines in

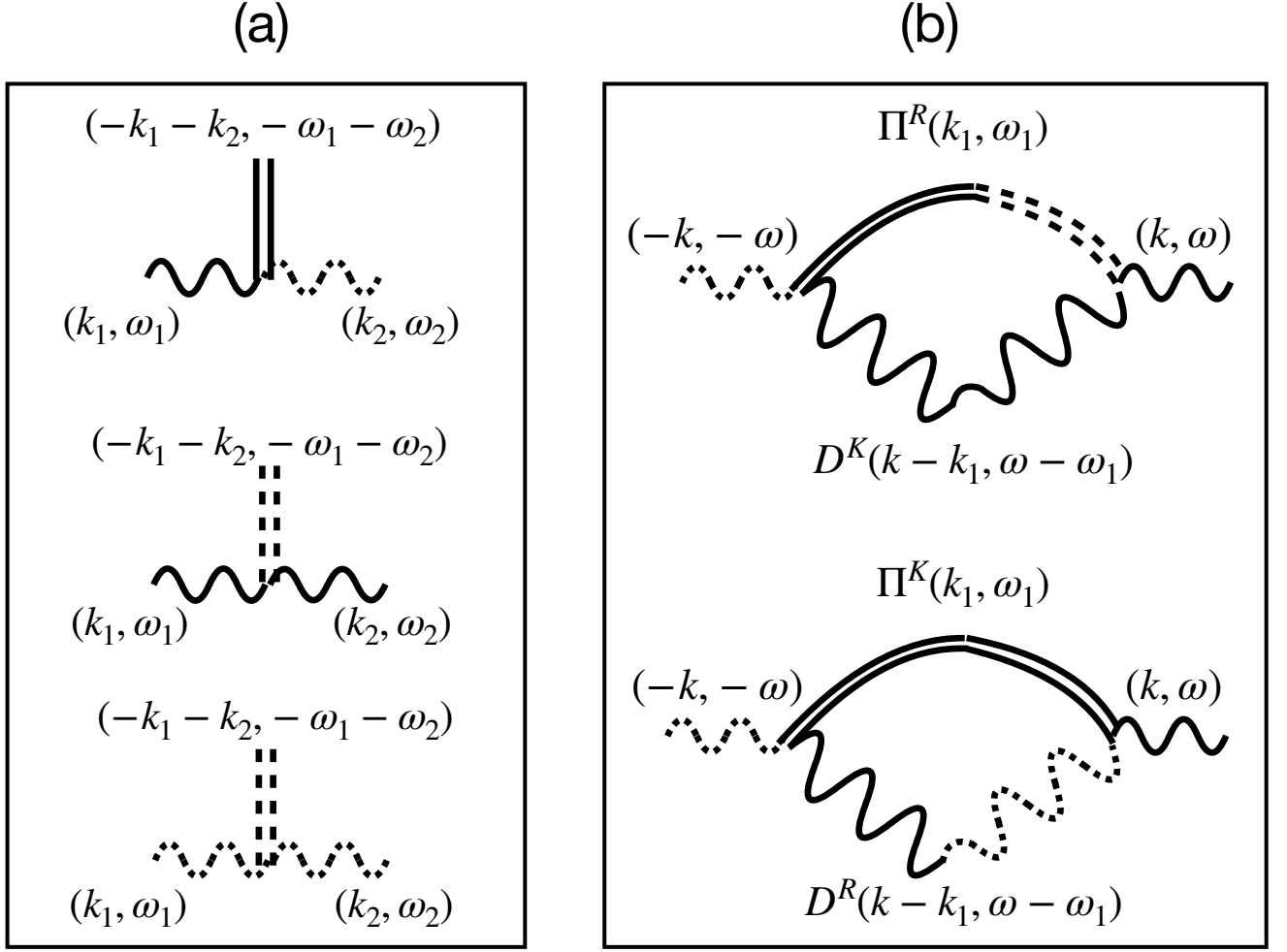


FIG. 8. Phonon relaxation due to two phonons scattering with fermions: (a) Allowed vertices for effective interaction between 2 phonons and particle-hole excitations. Solid (dashed) wavy lines are classical (quantum) phonon fields and solid (dashed) double lines are classical (quantum) particle-hole excitation fields. (b) Retarded self-energy diagrams for phonons: $D^{R/K}$ are phonon correlators (retarded/Keldysh components) and $\Pi^{R/K}$ are polarization functions (retarded/Keldysh components).

Fig. 6(b) are dressed by emission/absorption of phonons [an example is shown in Fig. 7 (a)] and (ii) diagrams where the fermionic polarization is dressed by vertex functions [an example is shown in Fig. 7 (b)]. The self-energy corrections of the fermion lines help in relaxing the energy-momentum constraints and are equivalent to the diagrams which lead to power laws in the earlier works⁷⁰; hence we will focus on them in this appendix and ignore the vertex corrections.

Let us focus on the diagram shown in Fig. 7(a). As we argued in the section on phonon self energy, the particle-hole pair with momenta $(k_2 + k_1, k_2 + k_1 - k)$ cannot satisfy energy-momentum conservation. However, the particle hole pair with momenta $(k_2 + k_1, k_2)$, together with the phonon at $(k - k_1)$ can satisfy the on-shell condition and give rise to a finite contribution to $\text{Im} \Sigma_{(4)}^R(k, \Omega_k)$. Note that the intermediate fermion at $k_2 + k_1 - k$ is necessarily off-shell. To make initial headway, and to compare with the earlier works, we replace these off-shell propagators by a constant (which we take to be 1, since we are interested in scaling of the decay rate). This effectively gives a 2-phonon, 2-fermion scattering vertex $\mathcal{O}(\kappa^4)$, similar to Ref. 70. We can also think of this as a vertex between two phonons and a particle-hole excitation. These effective vertices are shown in Fig. 8(a), where the double line represents a particle-hole propagator. The retarded self energy corrections for the phonons due to these effective vertices are shown in Fig. 8(b). The self energy is given by

$$\Sigma_{(4)}^R(k, \omega) = i\kappa^4 \lambda(k)^2 \int \frac{d\omega_1}{2\pi} \sum_{k_1} \lambda(k - k_1)^2 [D^R(k - k_1, \omega - \omega_1) \Pi^K(k_1, \omega_1) + D^K(k - k_1, \omega - \omega_1) \Pi^R(k_1, \omega_1)], \quad (\text{C2})$$

where λ is the form factor from the deformation potential, and $\Pi^{R/K}$ are polarization functions of the fermions which are also the

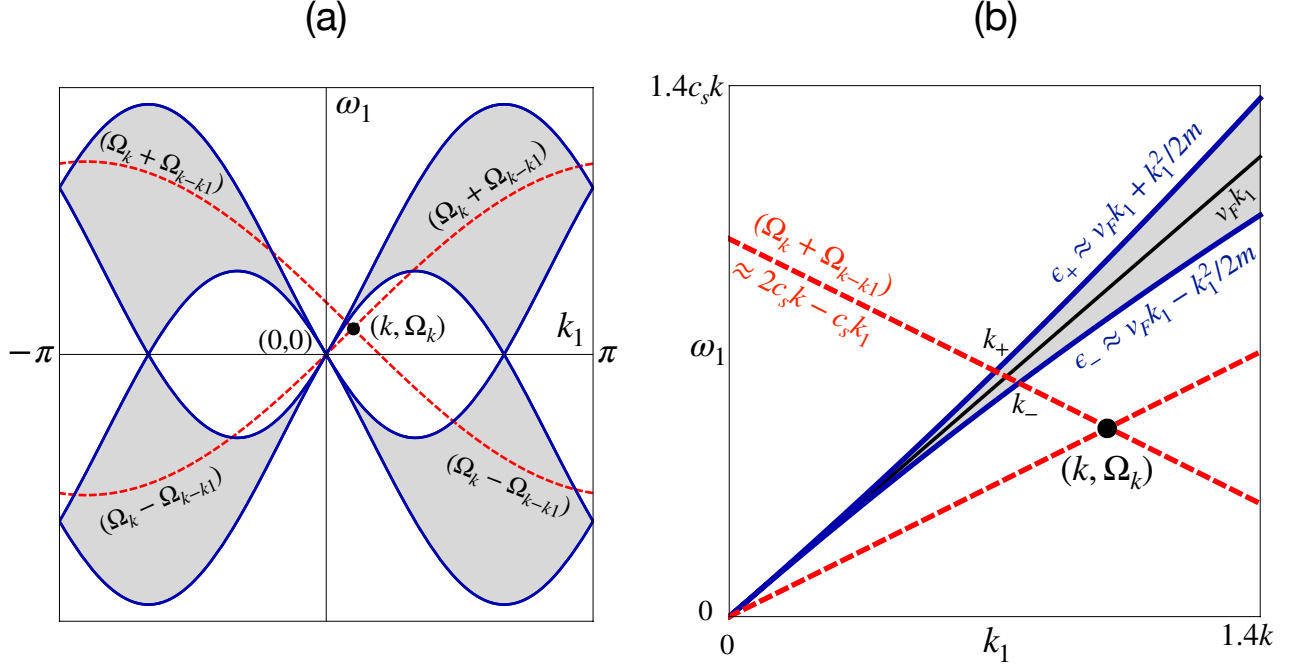


FIG. 9. Particle-hole continuum and contribution of 2-phonon processes to the decay rate (at momenta k): (a) The 1D particle-hole excitations have a finite spectral weight in the shaded region in k_1, ω_1 plane, bounded by solid blue lines. The dashed red lines correspond to the sum and difference of phonon energies, $\Omega_k + \Omega_{k-k_1}$ and $\Omega_k - \Omega_{k-k_1}$. The location (k, Ω_k) is shown as a solid black circle. The crossing of the red lines with the shaded regions indicate the values of (k_1, ω_1) which contributes to the self energy integral. For small k at low temperature, the contribution of the regions at large k_1 , where the phonon lines enter the particle hole continuum, is exponentially suppressed by thermal factors. (b) The small region at low values of k_1 , where the energy-momentum conditions are satisfied, is shown in detail. The shaded region, where particle-hole excitations have finite spectral weight, is around $v_F k$ and is bounded by $\epsilon_+ = v_F k + k_1^2/2m$ and $\epsilon_- = v_F k - k_1^2/2m$ (solid blue lines). The region of interest, where the phonon line crosses the shaded region, lies between k_+ and k_- , where $k_{\pm} \approx \frac{2c_s}{v_F + c_s} k \mp \frac{2c_s^2}{m(v_F + c_s)^3} k^2$.

particle-hole propagators. We note that solving the full non-equilibrium problem at this order is beyond the scope of this paper; however the calculation can be simplified by assuming thermal equilibrium, i.e. $D(\Pi)^K(p, \omega) = 2i \coth\left[\frac{\omega}{2T}\right] \text{Im} D(\Pi)^R(p, \omega)$, which is simply a statement of fluctuation dissipation theorem. The imaginary part of $\Sigma_{(4)}^R(k, \omega)$ is then given by

$$\text{Im} [\Sigma_{(4)}^R(k, \omega)] = -\kappa^4 \lambda(k)^2 \int \frac{d\omega_1}{\pi} \sum_{k_1} \lambda(k - k_1)^2 \left[\coth\left(\frac{\omega_1}{2T}\right) + \coth\left(\frac{\omega - \omega_1}{2T}\right) \right] \text{Im} D^R(k - k_1, \omega - \omega_1) \text{Im} \Pi^R(k_1, \omega_1). \quad (\text{C3})$$

Now, we are interested in the behaviour of this function at small k and $\omega = \Omega_k \sim c_s k$ (we assume $k, \Omega_k > 0$). In Fig. 9(a) we plot the region in k_1, ω_1 plane where the 1D particle-hole excitations have a finite spectral weight. This corresponds to the shaded area between the solid lines. The dashed lines correspond to the sum and difference of phonon energies, $\Omega_k + \Omega_{k-k_1}$ and $\Omega_k - \Omega_{k-k_1}$. The location (k, Ω_k) is shown as a solid circle in this figure. The crossing of the red lines with the shaded regions indicate the values of (k_1, ω_1) which contributes to the self energy integral. For small k at low temperature, the contribution of the regions at large k_1 , where the phonon lines enter the particle hole continuum, is exponentially suppressed by thermal factors. However there is a small region at low values of k_1 , where the energy-momentum conditions are satisfied, and this region contributes to the decay rate in the leading order. This region is shown in detail in Fig. 9(b), where the region of interest lies between k_+ and k_- , where $k_{\pm} \approx \frac{2c_s}{v_F + c_s} k \mp \frac{2c_s^2}{m(v_F + c_s)^3} k^2$. In this case, one can show that $\text{Im} \Pi^R(k_1, \omega_1) \sim \frac{-1}{|k_1|} \Theta[(\omega_1 - \epsilon_-)(\epsilon_+ - \omega_1)]$, where $\epsilon_+ = v_F k_1 + k_1^2/2m$ and $\epsilon_- = v_F k_1 - k_1^2/2m$. Here v_F is the Fermi velocity of the Fermi gas and m is the mass of the Fermions in the low energy long wavelength continuum description. Note that the width of this region $\sim k_1^2$ and is small at low k_1 . Further, the retarded phonon propagator has two poles at $\omega_1 = \Omega_k \pm \Omega_{k-k_1}$. From Fig. 9(b), we see that $\omega_1 > \Omega_k$ and hence

we only consider the residue of the propagator at $\omega_1 = \Omega_k + \Omega_{k-k_1}$. Putting all these together, we get

$$\text{Im} [\Sigma_{(4)}^R(k, c_s k)] \sim \frac{\kappa^4}{4} \lambda(k)^2 \int_{k_+}^{k_-} dk_1 \frac{\lambda(k-k_1)^2}{\Omega_{k-k_1}} \frac{1}{|k_1|} \left[\coth \left(\frac{c_s k + \Omega_{k-k_1}}{2T} \right) - \coth \left(\frac{\Omega_{k-k_1}}{2T} \right) \right], \quad (\text{C4})$$

For small k , we can replace the integration by the function value at $k_0 = \frac{1}{2}(k_+ + k_-) = \frac{2c_s}{v_F + c_s} k$ multiplied by the width of the region $\Delta k = \frac{4c_s^2}{m(v_F + c_s)^3} k^2$ to get the leading order estimate of $\text{Im} [\Sigma_{(4)}^R(k, c_s k)]$,

$$\begin{aligned} \text{Im} [\Sigma_{(4)}^R(k, c_s k)] &\sim \frac{\kappa^4}{4c_s} k^2 \frac{|k - k_0|}{|k_0|} \left[\coth \left(\frac{c_s k + \Omega_{k-k_0}}{2T} \right) - \coth \left(\frac{\Omega_{k-k_0}}{2T} \right) \right] \Delta k \\ &\sim -\kappa^4 \left(\frac{v_F - c_s}{2m(v_F + c_s)^3} \right) k^4 \left[\coth \left(\frac{v_F - c_s}{v_F + c_s} \frac{c_s k}{2T} \right) - \coth \left(\frac{2v_F}{v_F + c_s} \frac{c_s k}{2T} \right) \right]. \end{aligned} \quad (\text{C5})$$

We assume that v_F and c_s are of similar magnitude but $c_s < v_F$, so that $2v_F/(v_F + c_s) \sim 1$ and $(v_F - c_s)/(v_F + c_s) \sim 1$. In this case, for $T \ll c_s k$, the arguments of both the \coth functions in the above expression will be large and the value of each thermal factor will be exponentially (in inverse temperature) close to 1. So their difference will result in a decay rate which is exponentially small in inverse temperature, i.e. $\Gamma_k \sim k^3 e^{-c_s k/T}$. Note that if $v_F \gg c_s$, this argument is bolstered even more. For $T \gg c_s k$, the argument of the \coth functions are small, and we get $\Gamma_k \sim T k^2$.

The above calculations have neglected the energy momentum dependence of the off-shell fermionic propagators, which will give additional momentum dependence to the vertex between two phonons and particle-hole excitations. Since the energy mismatch (which determines how far off shell the fermionic propagators are) $\sim (v_F - c_s)k$, one would expect the fermion propagators to be $\sim \frac{1}{(v_F - c_s)k}$. This would reduce a factor of k^2 from the scaling. In this case, one would obtain $\Gamma_k \sim k e^{-c_s k/T}$ for $T \ll c_s k$ and $\Gamma_k \sim T$ for $T \gg c_s k$. Note that the high temperature result is equivalent to a standard thermal broadening, while the low T result is exponentially small rather than being a power law. This high T limit is similar to the case considered in Ref. 70 (where $\frac{k^2}{2m} \sim T$ for the single particle). In addition, the vertex in Ref. 70 does not have the extra $1/k$ factor from the off-shell fermion propagator.

We finally comment on why our calculations at the lowest temperatures show a different scaling of the decay rate from the earlier works^{70,71}. In the earlier works, which looks at scattering of single particles, the relevant momenta of fermions are close to 0 ($\sim \sqrt{T}$), while we are considering a Fermi sea at a finite density of fermions; so the fermions relevant for phonon relaxation in our case have momenta $\sim k_F$. Refs.70 and 71 considered the scattering of a massive particle which can be treated classically ($\frac{p^2}{2m} \sim T$). Since we have $c_s < v_F$, we do not have a temperature regime where the phonons are quantum but the relevant particle-hole excitations can be treated classically. Thus both degrees of freedom have quantum nature in our calculations. For low $T \ll c_s k$, the thermal factor in both the loss and gain rates in the collision integral approaches 1 to exponential accuracy. The leading order 1 is cancelled, leaving us with an exponentially small remaining term. This is the key reason the relaxation rate of phonons coupled to a Fermi sea in 1D remains exponential even when two phonon processes are considered, in contrast to the case of scattering of a single massive particle. Further the additional $1/k$ factors from the off-shell fermion lines change the power of k sitting in the prefactor to the exponential.

We also note that three-phonon processes involve two particle-hole excitations and satisfy energy-momentum conservation constraints. They can result in a decay rate which is polynomial in temperature and hence not exponentially small. However, these processes are of $\mathcal{O}(\kappa^8)$ and for small system-bath coupling they are suppressed.

Appendix D: Characterization of polarinon mode in 1D

In this appendix we will discuss some details about the undamped polarinon mode situated just outside particle-hole band edge. We noticed (as discussed in Section III B 1) that particle-hole DOS has inverse square root divergence near band edge in 1D. Using Kramers-Kronig relations⁹⁶ one can show that the real part of the retarded self energy diverges in the same way just outside the particle-hole band edge [see Fig. 3(e)].

Now, for the pole of the inverse Green's function outside the particle-hole band edge we have the equation

$$\omega^2 - \Omega_k^2 - \frac{g(k, \omega)}{\sqrt{\omega - \omega_{max}(k)}} = 0, \quad (\text{D1})$$

where we have assumed $\Sigma^R(k, \omega) \sim \frac{2g(k, \omega)}{\sqrt{\omega - \omega_{max}(k)}}$ and $g(k, \omega)$ is a function of k and ω (also depends on the bath parameters) but varies slowly with ω as we have separated out the divergent piece. We also considered a phonon mode below the particle-hole band edge so that $\Omega_k < \omega_{max}(k)$.

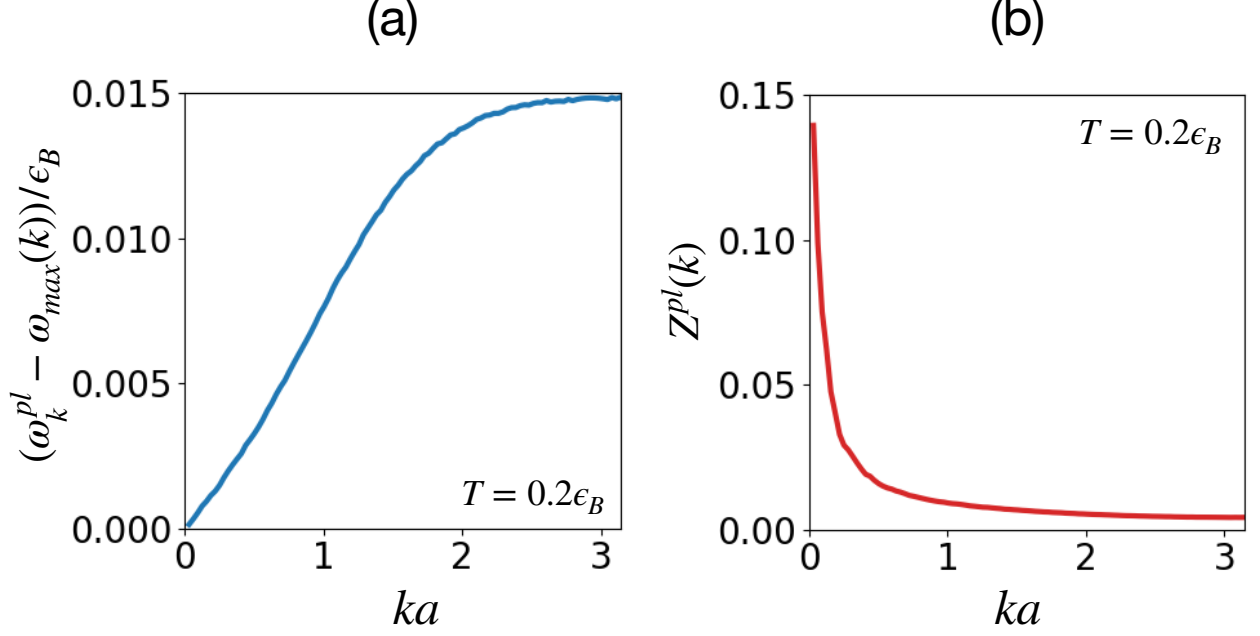


FIG. 10. Specifications of “polarinon” modes. (a) Distance of the polarinon modes from particle-hole band edge is plotted as a function of momenta. It increases smoothly with momenta. (b) Spectral weight of the polarinon modes is plotted as a function of momenta. The weight falls sharply with momenta. Hence the polarinon modes will not affect the dynamics of the phonons at higher momenta. The bath is set at $T = 0.2\epsilon_B$ and $\mu = 0.5\epsilon_B$. The system-bath coupling strength is $\kappa^2 = 0.9\epsilon_B^3 a$.

Now we define $x = \omega - \omega_{max}(k)$. For small positive x , the solution of Eq. (D1) becomes

$$x(k) = \frac{[g(k, \omega_{max}(k))]^2}{(\omega_{max}(k)^2 - \Omega_k^2)^2}. \quad (D2)$$

The spectral weight of this mode is given by

$$Z^{pl}(k) \approx \frac{[x(k)]^{3/2}}{g(k, \omega_{max}(k))} = \frac{[g(k, \omega_{max}(k))]^2}{(\omega_{max}(k)^2 - \Omega_k^2)^3}. \quad (D3)$$

We have $\omega_{max} = 2\epsilon_B |\sin(ka/2)|$ and $\Omega_k = \omega_0 |\sin(ka/2)|$ where $2\epsilon_B$ is the fermion bandwidth and ω_0 is the phonon bandwidth. For the electron-phonon coupling we have considered, we can separate out leading k -dependence of g as $g(k, \omega_{max}(k)) = \sin^2(ka/2)f(k)$, where $f(k)$ is a smooth function. With these inputs we have

$$x(k) = \frac{1}{[4\epsilon_B^2 - \omega_0^2]^2} [f(k)]^2 \quad (D4)$$

$$Z^{pl}(k) = \frac{1}{[4\epsilon_B^2 - \omega_0^2]^2} \left[\frac{f(k)}{\sin(k/2)} \right]^2. \quad (D5)$$

We have calculated $x(k)$ and $Z^{pl}(k)$ numerically and plotted them as a function of momenta k at bath temperature $T = 0.2\epsilon_B$ and chemical potential $\mu = 0.5\epsilon_B$ in Fig. 10. The system-bath coupling strength is $\kappa^2 = 0.9\epsilon_B^3 a$. We note that their behaviour is consistent with the analytical forms [see Eq. D4]. While $x(k)$ increases with k , $Z^{pl}(k)$ falls sharply with k and hence they have little role to play in the dynamics of the phonons at higher momenta.

* mursalin@theory.tifr.res.in

¹ F. Englert and R. Brout, *Phys. Rev. Lett.* **13**, 321 (1964).

- ² P. Higgs, *Physics Letters* **12**, 132 (1964).
- ³ P. W. Higgs, *Phys. Rev. Lett.* **13**, 508 (1964).
- ⁴ A. R. Liddle, in *ICTP Summer School in High-Energy Physics and Cosmology* (World Scientific, Singapore, 1999) [arXiv:astro-ph/9901124](https://arxiv.org/abs/astro-ph/9901124).
- ⁵ B. A. Bassett, S. Tsujikawa, and D. Wands, *Rev. Mod. Phys.* **78**, 537 (2006).
- ⁶ J. Magaña and T. Matos, *Journal of Physics: Conference Series* **378**, 012012 (2012).
- ⁷ L. Hui, J. P. Ostriker, S. Tremaine, and E. Witten, *Phys. Rev. D* **95**, 043541 (2017).
- ⁸ F. Chadha-Day, J. Ellis, and D. J. E. Marsh, “Axion dark matter: What is it and why now?” (2021), [arXiv:2105.01406 \[hep-ph\]](https://arxiv.org/abs/2105.01406).
- ⁹ S. Doniach and E. H. Sondheimer, *Green’s Functions for Solid State Physicists* (Imperial College press, London, UK, 1998).
- ¹⁰ C. E. Patton, *Physics Reports* **103**, 251 (1984).
- ¹¹ P. W. Anderson, *Rev. Mod. Phys.* **38**, 298 (1966).
- ¹² A. Schmitt, *Introduction to Superfluidity* (Springer International Publishing, Switzerland, 2015).
- ¹³ G. Rempe, R. J. Thompson, R. J. Brecha, W. D. Lee, and H. J. Kimble, *Phys. Rev. Lett.* **67**, 1727 (1991).
- ¹⁴ R. J. Thompson, G. Rempe, and H. J. Kimble, *Phys. Rev. Lett.* **68**, 1132 (1992).
- ¹⁵ R. Miller, T. E. Northup, K. M. Birnbaum, A. Boca, A. D. Boozer, and H. J. Kimble, *Journal of Physics B: Atomic, Molecular and Optical Physics* **38**, S551 (2005).
- ¹⁶ H. Walther, B. T. H. Varcoe, B.-G. Englert, and T. Becker, *Reports on Progress in Physics* **69**, 1325 (2006).
- ¹⁷ L. Tonks and I. Langmuir, *Phys. Rev.* **33**, 195 (1929).
- ¹⁸ K. Tolpygo, *Ukr. J. Phys.* **53**, 93 (2008).
- ¹⁹ K. Huang, *Nature* **167**, 779 (1951).
- ²⁰ D. L. Mills and E. Burstein, *Reports on Progress in Physics* **37**, 817 (1974).
- ²¹ D. N. Basov, A. Asenjo-Garcia, P. J. Schuck, X. Zhu, and A. Rubio, *Nanophotonics* **10**, 549 (2021).
- ²² M. E. Peskin and D. V. Schroeder, *An Introduction to quantum field theory* (Addison-Wesley, Reading, USA, 1995).
- ²³ M. Srednicki, *Quantum Field Theory* (Cambridge University Press, Cambridge, UK, 2007).
- ²⁴ A. Altland and B. D. Simons, *Condensed Matter Field Theory*, 2nd ed. (Cambridge University Press, Cambridge, UK, 2010).
- ²⁵ E. Calzetta and B. L. Hu, *Phys. Rev. D* **37**, 2878 (1988).
- ²⁶ J. Berges, *Nuclear Physics A* **699**, 847 (2002).
- ²⁷ A. Anisimov, W. Buchmüller, M. Drewes, and S. Mendizabal, *Annals of Physics* **324**, 1234 (2009).
- ²⁸ K. Mukaida and K. Nakayama, *Journal of Cosmology and Astroparticle Physics* **2013**, 017 (2013).
- ²⁹ C. Thomsen, H. T. Grahn, H. J. Maris, and J. Tauc, *Phys. Rev. B* **34**, 4129 (1986).
- ³⁰ J. Qi, X. Chen, W. Yu, P. Cadden-Zimansky, D. Smirnov, N. H. Tolk, I. Miotkowski, H. Cao, Y. P. Chen, Y. Wu, S. Qiao, and Z. Jiang, *Applied Physics Letters* **97**, 182102 (2010).
- ³¹ D. Novko, F. Caruso, C. Draxl, and E. Cappelluti, *Phys. Rev. Lett.* **124**, 077001 (2020).
- ³² P.-A. Mante, L. Belliard, and B. Perrin, *Nanophotonics* **7**, 1759 (2018).
- ³³ H. Kawashima, M. M. Wefers, and K. A. Nelson, *Annual Review of Physical Chemistry* **46**, 627 (1995), pMID: 24341370.
- ³⁴ A. Weiner and A. Kan’an, *IEEE Journal of Selected Topics in Quantum Electronics* **4**, 317 (1998).
- ³⁵ M. Fetterman, D. Goswami, D. Keusters, W. Yang, J.-K. Rhee, and W. Warren, *Opt. Express* **3**, 366 (1998).
- ³⁶ A. M. Weiner, *Review of Scientific Instruments* **71**, 1929 (2000).
- ³⁷ A. M. Weiner, *Optics Communications* **284**, 3669 (2011), special Issue on Optical Pulse Shaping, Arbitrary Waveform Generation, and Pulse Characterization.
- ³⁸ P. Ginzburg, *Reviews in Physics* **1**, 120 (2016).
- ³⁹ K. Weiher, E. Agudelo, and M. Bohmann, *Phys. Rev. A* **100**, 043812 (2019).
- ⁴⁰ A. Dey and M. Kulkarni, *Phys. Rev. A* **101**, 043801 (2020).
- ⁴¹ O. c. v. Černotík, A. Dantan, and C. Genes, *Phys. Rev. Lett.* **122**, 243601 (2019).
- ⁴² R. Loudon and P. Knight, *Journal of Modern Optics* **34**, 709 (1987).
- ⁴³ A. I. Lvovsky, “Squeezed light,” [arXiv:1401.4118 \[quant-ph\]](https://arxiv.org/abs/1401.4118).
- ⁴⁴ E. A. Sete, H. Eleuch, and S. Das, *Phys. Rev. A* **84**, 053817 (2011).
- ⁴⁵ D. Q. Bao, C. J. Zhu, Y. P. Yang, and G. S. Agarwal, *Opt. Express* **27**, 15540 (2019).
- ⁴⁶ J. Schwinger, *Journal of Mathematical Physics* **2**, 407 (1961).
- ⁴⁷ L. V. Keldysh, *Sov. Phys. JETP* **20**, 1018 (1965).
- ⁴⁸ A. Kamenev and A. Levchenko, *Advances in Physics* **58**, 197 (2009).
- ⁴⁹ A. Kamenev, *Field Theory of Non-Equilibrium Systems* (Cambridge University Press, New York, 2011).
- ⁵⁰ J. Rammer, *Quantum Field Theory of Non-equilibrium States* (Cambridge University Press, New York, 2007).
- ⁵¹ A. Chakraborty, P. Gorantla, and R. Sensarma, *Phys. Rev. B* **99**, 054306 (2019).
- ⁵² A. J. Leggett, S. Chakravarty, A. T. Dorsey, M. P. A. Fisher, A. Garg, and W. Zwerger, *Rev. Mod. Phys.* **59**, 1 (1987).
- ⁵³ C. Gardiner and P. Zoller, *Quantum Noise* (Springer Berlin, Heidelberg).
- ⁵⁴ H. E. Elsayed-Ali, T. B. Norris, M. A. Pessot, and G. A. Mourou, *Phys. Rev. Lett.* **58**, 1212 (1987).
- ⁵⁵ F. C. Wellstood, C. Urbina, and J. Clarke, *Phys. Rev. B* **49**, 5942 (1994).
- ⁵⁶ N. Del Fatti, C. Voisin, M. Achermann, S. Tzortzakias, D. Christofilos, and F. Vallée, *Phys. Rev. B* **61**, 16956 (2000).
- ⁵⁷ F. Giazotto, T. T. Heikkilä, A. Luukanen, A. M. Savin, and J. P. Pekola, *Rev. Mod. Phys.* **78**, 217 (2006).
- ⁵⁸ A. Habib, F. Florio, and R. Sundararaman, *Journal of Optics* **20**, 064001 (2018).
- ⁵⁹ F. S. Bergeret, M. Silaev, P. Virtanen, and T. T. Heikkilä, *Rev. Mod. Phys.* **90**, 041001 (2018).
- ⁶⁰ S. Dal Forno and J. Lischner, *Phys. Rev. Materials* **3**, 115203 (2019).
- ⁶¹ C. Giannetti, M. Capone, D. Fausti, M. Fabrizio, F. Parmigiani, and D. Mihailovic, *Advances in Physics* **65**, 58 (2016).
- ⁶² L. V. Besteiro, E. Cortés, S. Ishii, P. Narang, and R. F. Oulton, *Journal of Applied Physics* **129**, 150401 (2021).
- ⁶³ T. Peterreins, J. Jochum, F. Pröbst, F. V. Feilitzsch, H. Kraus, and R. L. Mössbauer, *Journal of Applied Physics* **69**, 1791 (1991).
- ⁶⁴ J. B. Hertzberg, O. O. Otelaja, N. J. Yoshida, and R. D. Robinson, *Review of Scientific Instruments* **82**, 104905 (2011).
- ⁶⁵ E. Perinati, M. Barbera, A. Collura, S. Serio, and E. Silver, *Nuclear Instruments and Methods in Physics Research Section A: Accelerators, Spectrometers, Detectors and Associated Equipment* **531**, 459 (2004).
- ⁶⁶ M. Zukerstein, F. Trojánek, B. Rezek, Z. Šobáň, M. Kozák, and P. Malý, *Applied Physics Letters* **115**, 161104 (2019).
- ⁶⁷ M. Lakehal, M. Schiró, I. M. Eremin, and I. Paul, *Phys. Rev. B* **102**, 174316 (2020).
- ⁶⁸ T. Micklitz, J. Rech, and K. A. Matveev, *Phys. Rev. B* **81**, 115313 (2010).
- ⁶⁹ K. A. Matveev, A. V. Andreev, and M. Pustilnik, *Phys. Rev. Lett.* **105**, 046401 (2010).
- ⁷⁰ A. H. Castro Neto and M. P. A. Fisher, *Phys. Rev. B* **53**, 9713

- (1996).
- ⁷¹ D. M. Gangardt and A. Kamenev, *Phys. Rev. Lett.* **102**, 070402 (2009).
- ⁷² S. Pekar, *Journal of Physics and Chemistry of Solids* **5**, 11 (1958).
- ⁷³ C. Weisbuch, M. Nishioka, A. Ishikawa, and Y. Arakawa, *Phys. Rev. Lett.* **69**, 3314 (1992).
- ⁷⁴ N. OCKMAN, W. WANG, and R. ALFANO, *International Journal of Modern Physics B* **05**, 3165 (1991).
- ⁷⁵ J. Flock, T. Dekorsy, and O. V. Misochko, *Applied Physics Letters* **105**, 011902 (2014).
- ⁷⁶ J. Hu, K. Igarashi, T. Sasagawa, K. G. Nakamura, and O. V. Misochko, *Applied Physics Letters* **112**, 031901 (2018).
- ⁷⁷ W. Busza, K. Rajagopal, and W. van der Schee, *Annual Review of Nuclear and Particle Science* **68**, 339 (2018).
- ⁷⁸ A. Mitra, *Annual Review of Condensed Matter Physics* **9**, 245 (2018).
- ⁷⁹ S. R. Das, D. A. Galante, and R. C. Myers, *Journal of High Energy Physics* **2016** (2016), 10.1007/jhep05(2016)164.
- ⁸⁰ G. Mandal, S. Paranjape, and N. Sorokhaibam, “Thermalization in 2d critical quench and uv/ir mixing,” (2020), arXiv:1512.02187 [hep-th].
- ⁸¹ G. N. Watson, *Journal of the London Mathematical Society* **s1-8**, 194 (1933).
- ⁸² U. Weiss, *Quantum Dissipative Systems*, 3rd ed. (World Scientific, Singapore, 2008).
- ⁸³ A. Chakraborty and R. Sensarma, *Phys. Rev. B* **97**, 104306 (2018).
- ⁸⁴ H. G. Dawson, *Proceedings of the London Mathematical Society* **s1-29**, 519 (1897).
- ⁸⁵ A. A. Abrikosov, L. P. Gorkov, I. E. Dzyaloshinski, and R. A. Silverman, *Methods of Quantum Field Theory in Statistical Physics* (Dover, New York, 1975).
- ⁸⁶ F. Giustino, *Rev. Mod. Phys.* **89**, 015003 (2017).
- ⁸⁷ J.-M. Lai, Y.-R. Xie, and J. Zhang, *Nano Research* **14**, 1711 (2021).
- ⁸⁸ Z. Huang, W. Zhou, J. Huang, J. Wu, Y. Gao, Y. Qu, and J. Chu, *Scientific Reports* **6**, 22938 (2016).
- ⁸⁹ H. Yu, Y. Peng, Y. Yang, and Z.-Y. Li, *npj Computational Materials* **5**, 45 (2019).
- ⁹⁰ H. Ritsch, P. Domokos, F. Brennecke, and T. Esslinger, *Rev. Mod. Phys.* **85**, 553 (2013).
- ⁹¹ E. Massó, F. Rota, and G. Zsembinszki, *Phys. Rev. D* **66**, 023004 (2002).
- ⁹² G. D. Mahan, *Many-Particle Physics* (Springer New York, 2000).
- ⁹³ T. Giamarchi, *Quantum physics in one dimension* (Oxford University Press, New York, 2003).
- ⁹⁴ L. Yang, Y. Tao, J. Liu, C. Liu, Q. Zhang, M. Akter, Y. Zhao, T. T. Xu, Y. Xu, Z. Mao, Y. Chen, and D. Li, *Nano Letters* **19**, 415 (2019).
- ⁹⁵ R. Hoffmann, S. Shaik, J. Scott, M.-H. Whangbo, and M. J. Foshee, *Journal of Solid State Chemistry* **34**, 263 (1980).
- ⁹⁶ G. B. Arfken, H. J. Weber, and F. E. Harris, in *Mathematical Methods for Physicists (Seventh Edition)*, edited by G. B. Arfken, H. J. Weber, and F. E. Harris (Academic Press, Boston, 2013) seventh edition ed., pp. 551–598.
- ⁹⁷ I. Pletikosić, M. N. Ali, A. V. Fedorov, R. J. Cava, and T. Valla, *Phys. Rev. Lett.* **113**, 216601 (2014).
- ⁹⁸ J. Jiang, F. Tang, X. C. Pan, H. M. Liu, X. H. Niu, Y. X. Wang, D. F. Xu, H. F. Yang, B. P. Xie, F. Q. Song, P. Dudin, T. K. Kim, M. Hoesch, P. K. Das, I. Vobornik, X. G. Wan, and D. L. Feng, *Phys. Rev. Lett.* **115**, 166601 (2015).
- ⁹⁹ L.-K. Zeng, R. Lou, D.-S. Wu, Q. N. Xu, P.-J. Guo, L.-Y. Kong, Y.-G. Zhong, J.-Z. Ma, B.-B. Fu, P. Richard, P. Wang, G. T. Liu, L. Lu, Y.-B. Huang, C. Fang, S.-S. Sun, Q. Wang, L. Wang, Y.-G. Shi, H. M. Weng, H.-C. Lei, K. Liu, S.-C. Wang, T. Qian, J.-L. Luo, and H. Ding, *Phys. Rev. Lett.* **117**, 127204 (2016).
- ¹⁰⁰ E. McCann and M. Koshino, *Reports on Progress in Physics* **76**, 056503 (2013).
- ¹⁰¹ S. Das Sarma, E. H. Hwang, and E. Rossi, *Phys. Rev. B* **81**, 161407(R) (2010).
- ¹⁰² O. Vafek and K. Yang, *Phys. Rev. B* **81**, 041401(R) (2010).
- ¹⁰³ N. W. Ashcroft and N. D. Mermin, *Solid State Physics* (Holt-Saunders, Philadelphia, 1976).